JOURNAL OF GEOPHYSICAL RESEARCH, VOL. 105, NO. C9, PAGES 21,893-21,911, SEPTEMBER 15, 2000

Surface currents in the Canary Basin from drifter observations

Meng Zhou
Large Lakes Observatory, University of Minnesota, Duluth

Jeffrey D. Paduan
Department of Oceanography, Naval postgraduate School, Monterey

Pearn P.Niiler
Scripps Institution of Oceanography, University of California, San Diego, La Jolla

Abstract. Satellite-tracked drifting buoys, deployed in the Canary Basin as part of the Subduction Experiment between July 1991 and October 1993 and the French Semaphore Experiment during October 1993, were used to obtain a description of surface currents and temperature in the Canary Basin. The study focuses on surface water convergence, eddy energy production, and heat transport. The Azores Current associated with the subtropical convergence zone is clearly visible at 34°N, and bifurcates around 22°W, with the major branch of the current circling the Madeira plateau and joining the Canary Current along the continental slope. Eddy kinetic energy maxima are found along the Azores Current. The mean current revealed a region of maximum convergence north of the Azores Current around longitude 29°W occurring with a negative heating anomaly and positive work done by the Reynolds stress. The southward meridional temperature fluxes in the Ekman layer (0-50 m) between 37°W and the African and European coast are estimated between $-0.076 \pm 0.022 \times 10^{15}$ W, produced by mean southward volume transport in our study area. The residual between local surface heat fluxes and horizontal convergence of heat implies a vertical heat convergence process associated with mesoscale temperature and flow fields.

1. Introduction

Surface circulation and air-sea heat exchange in the Canary Basin of the northeast Atlantic are believed to play a controlling role in the formation and movement of intermediate depth water masses. *Luyten, et al.* [1983] described the thermocline ocean currents by applying potential vorticity conservation to the layers beneath the turbulent surface ocean. In their theory the deeper flow is constrained by the layer thickness in outcrop regions where isopycnals intersect the surface. Deep isopycnals form much of the tropical and southern Atlantic outcrop in the Canary Basin, which is why surface ocean processes in that region can have far-reaching influences.

Much can be learned about deep-ocean circulation by observing density distributions in the northeast Atlantic. It will not be possible, however, to describe variations in the currents, or to predict the long-term effect of climatic shifts in surface conditions, until links are established between the seasonally modulated surface ocean and the layer thickness below it. How is fluid exchanged between the heated or cooled mixed layer and the main thermocline? It is hypothesized that lenses of cooled water in the deepest parts of the late-winter mixed layer become isolated from surface forcing by the formation of the seasonal thermocline [*de Szoeke*, 1980; *Federiuk and Price*, 1984; *Cushman-Roisin*, 1987; *Nurser and Marshall*, 1991]. Also, the outcropping region exists beneath the region of mean downwelling wind stress curl [*Isemer and Hasse*, 1987; *Huang*, 1990]. Coupled convection and Ekman pumping may play central roles in fluid export to the thermocline, known as subduction, but details of subduction processes are not available from Sverdrup-like theories.

An alternative to the notion of subduction processes driven by broad, weak Ekman pumping is the possibility that downwelling concentrated along fronts is responsible for the integrated effects observed below the surface layer [*Pollard and Regier*, 1990, 1992; *Rudnick and Luyten*, 1996]. Subduction associated with eddy dynamics around fronts is larger than Ekman convergence. In the Canary Basin, the subtropical front exists around 34°N and the current associated with the eastward flow along it is known as the Azores Current [*Käse and Siedler*, 1982; *Pollard and Pu*, 1985; *Klein and Sielder*, 1989]. If frontal processes are important to subduction, then surface circulation and heat fluxes around the Azores Front should be examined in detail.

A concentrated field study of the surface and thermocline waters of the Canary Basin was initiated by the Office of Naval Research in 1991, known as the Subduction Experiment. This study supported a variety of short-term and long-term measurement systems. It included observations designed to study flow in the potential-vorticity-conserving deeper layers, such as floats and tracers, and observations designed to study convergence in the Ekman layer, such as an array of meteorological moorings and large numbers of surface drifters. High-resolution surveys using a SeaSoar (Chelsea

Paper number 2000JC900096.
0148-0227/00/2000JC900096$09.00

Instruments, East Molesey, Surrey, England) were conducted across the Azores Front in an attempt to describe secondary circulation associated with the front. *Rudnick and Luyten* [1996] provided evidence of cold water from the north being subducted beneath the front.

A French air-sea interaction experiment (Semaphore) was also conducted in the northern Canary Basin in 1993 focusing on the Azeros Current, its meanders, meddies, and air-sea interaction [*Eymard et al.*, 1996; *Caniaux and Planton*, 1998; *Eymard*, 1998; *Kwon et al.*, 1998; *Richardson and Tychensky*, 1998; *Tychensky et al.*, 1998]. Observations provided new insights into fine-scale dynamics of the Azores Current. Results revealed that in the northwest of the Azores Current a meddy was coupled to a subsurface anticyclone and interacted with the Azores Current, creating a large-amplitude northward meander by vertical alignment of vorticity. In the southeast of the Azores Current, another meddy was vertically aligned with an anticyclonic meander of the Azores Current. Evidence demonstrated that the large meridional meanders associated with the Azores Current interact with the meddies.

Satellite-tracked drifting buoys were deployed in the Canary Basin as part of the Subduction Experiment between July 1991 and October 1993. Additional drifting buoys were deployed by the French air-sea interaction experiment called Semaphore [*Eymard et al.*, 1996] and by the World Ocean Circulation Experiment's Surface Velocity Program (WOCE/SVP). Repeated deployments were made on both sides of the climatological position of the Azores Front with goals of mapping the mixed layer mean velocity and temperature fields and computing the convergence and heat fluxes associated with mean circulation and mesoscale eddy fields. The suggestion of a regular pattern of convergence on the northern side and divergence on the southern side of the subtropical front in the North Pacific is evident in the drifter observations of *Niiler and Reynolds* [1984]. The repeated, multi-year deployments in the Subduction Experiment were designed to obtain a statistically significant confirmation of such a pattern in the northeast Atlantic Ocean.

This paper describes the surface processes in the Canary Basin based on drifter observations between July 1991 and March 1995. The study area is outlined in Figure 1, which shows bathymetric contours of the northeast Atlantic Ocean together with locations of the Azores, Madeira, and Canary Islands for reference. The drifters used in the study and their distribution of data by locations and seasons are shown in section 2. The regional view of mean currents, eddy kinetic energies, and eddy diffusivity are shown in section 3. Sea level anomaly calculations are in section 4. Relative vorticity, convergence, and kinetic energy fluxes are shown in section 5. Estimates of thermal energy fluxes using temperature measurements by drifters are shown in section 6. A discussion and summary are presented in section 7.

2. Data

The drifters used in this study were all mixed-layer drifters that conformed to WOCE standards in which drogue elements centered at 15 m provide for the drag area ratio great than 40. All of the drifters are known to follow water motion at 15 m within 1 cm s^{-1} error in wind conditions up to 10 m s^{-1} [*Sybrandy and Niiler*, 1991; *Niiler et al.*, 1987, 1995]. Drifters were tracked using the Argos Data Collection and Location System (ARGOS+) onboard polar-orbiting satellites. This system, as operated by Service Argos, provides position information with a minimum error of 300 m. In this study area, *Giannetti* [1993] determined the standard deviations of drifter locations were 383 m in the east-west direction and 359 m in the north-south direction based on positions

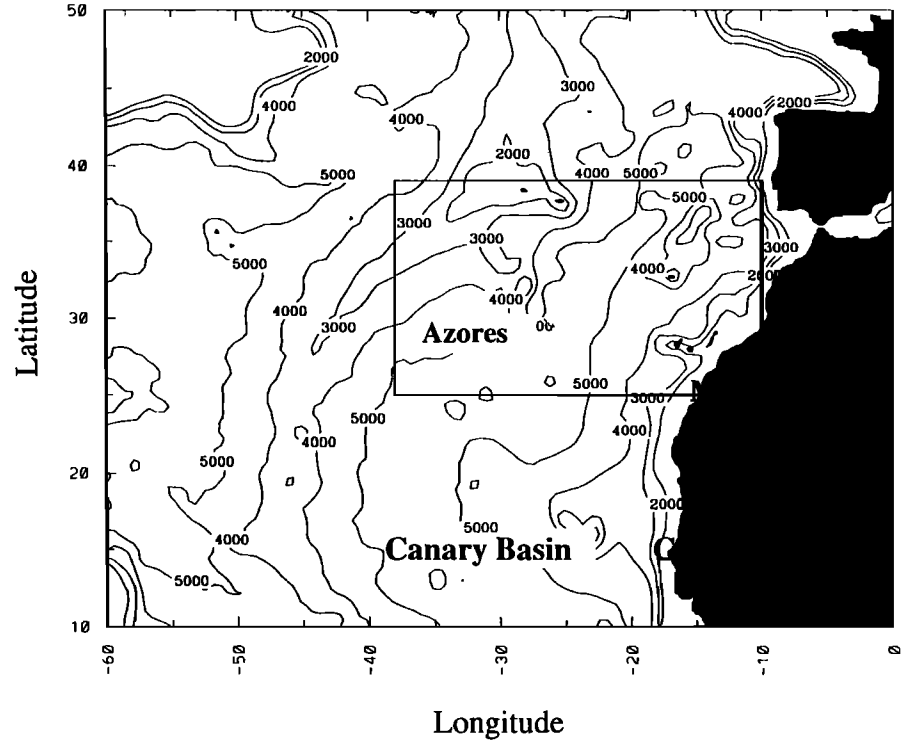

Figure 1. Area map and bathymetry. The contour interval is equal to 1000 m.

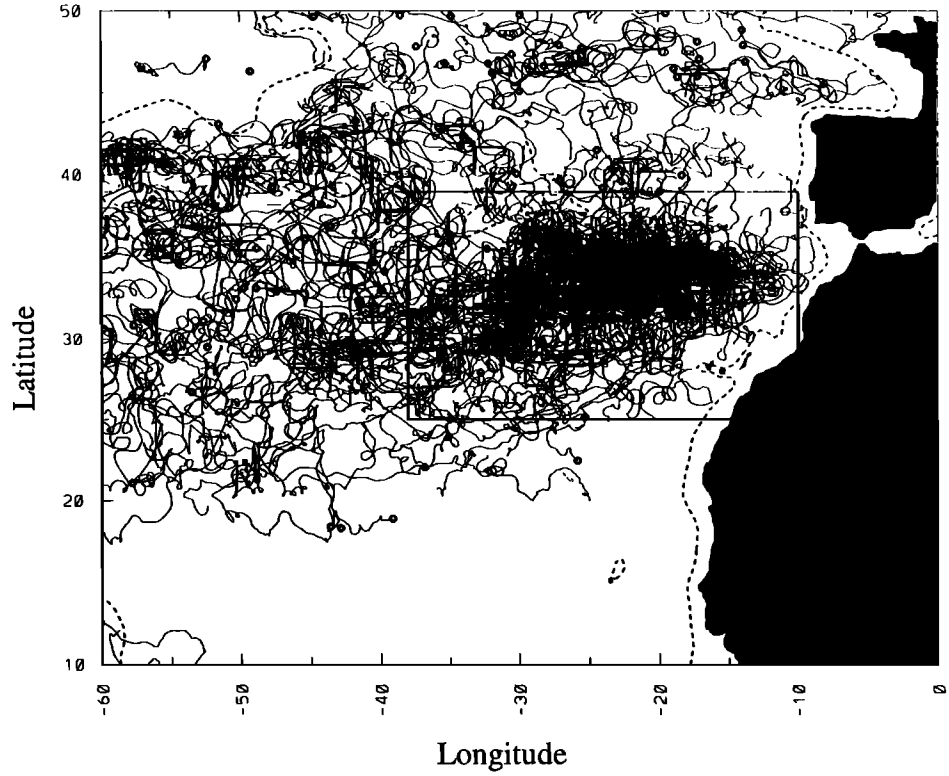

Figure 2. Composite trajectories from WOCE-standard drifters with drogues at 15 m in the northeast Atlantic Ocean. Our study area is boxed between 25°N, 38°W and 39°N, 10°W. Thick circles and lines denote deployment locations and trajectories of drifters. Heavy dashed contours show the 2000-m isobath.

received over several months from a drifter stranded on São Jorge Island. The position of a drifter was further interpolated to positions every 6 hours based on optimal interpolation [*Hansen and Poulain*, 1996]. If we assume the maximum positioning error between two daily fixes is not greater than 800 m, twice the standard deviation, the error of a daily averaged current is expected to be less than 1 cm s^{-1}, commensurate with the uncertainty due to drogue slippage.

In order to save tracking costs, most of the drifters used in this study were programmed to transmit only 1 day out of 3. On average, eight position fixes of a drifter were received during these 1-day operating periods. Initially, the raw ARGOS positions and sea surface temperature (SST) from each drifter were quality-controlled and interpolated to a uniform 6-hourly time series by the SVP Data Assembly Center at National Oceanic and Atmospheric Administration/Atlantic Oceanographic and Meteorological Laboratory (NOAA/AOML) in Miami, Florida. These interpolations were done according to the method of *Hansen and Poulain* [1996]. Because of the transmitter duty cycle and the processing applied to drifter data, there is no possibility of resolving high-frequency fluctuations due to tides or inertial currents. Even though the drifter data were interpolated at a temporal resolution of 6 hours, the time interval between two independent measurements is not less than 2 days dictated by the transmitter duty cycle.

A spatial overview of the surface drifter data in the Canary Basin is given in Figure 2, which shows the composite of all trajectories for the period of July 1991 through March 1995. Deployment locations are denoted by thick circles and the region described in this study is outlined by the box between 38°W, 25°N and 10°W, 39°N. The temporal distribution of drifter sampling is shown in Figure 3, indicating both the lifetime of individual drifters with drogues and the number of daily observations within the study area by month. A total of 122 drifters are represented in Figures 2 and 3. Deployments in groups of five were made nominally by volunteer research vessels every few months, and a large deployment of drifters was made in October 1993 in conjunction with Semaphore. Because of the long lifetime of instruments and the concentrated deployments in fall 1993, the observations peaked at 1500 daily observations per month from October 1993 through May 1994. More than 500 daily observations per month were obtained in the study area throughout the 3-year period from February 1992 to March 1995.

Many of the results obtained in this study are based on ensemble averages of drifter data within geographical 1° latitude × 2° longitude subregions. We will show that this box size provides for statistically reliable mean values over much of the study area while still providing enough resolution to map the variability of dynamical processes. The spatial distribution of daily observations in those 1° latitude × 2° longitude subregions is shown in(Figure 4).Typically, daily observations ranged between 300 and 600, with a maximum of 900, in the area around 35°N, 23°W.

3. Mean Current Descriptions

Our goal here is to present mean values of surface circulation that are representative of annual average processes in the Canary Basin. The statistical reliability of mean values determined from drifter observations is limited by variability

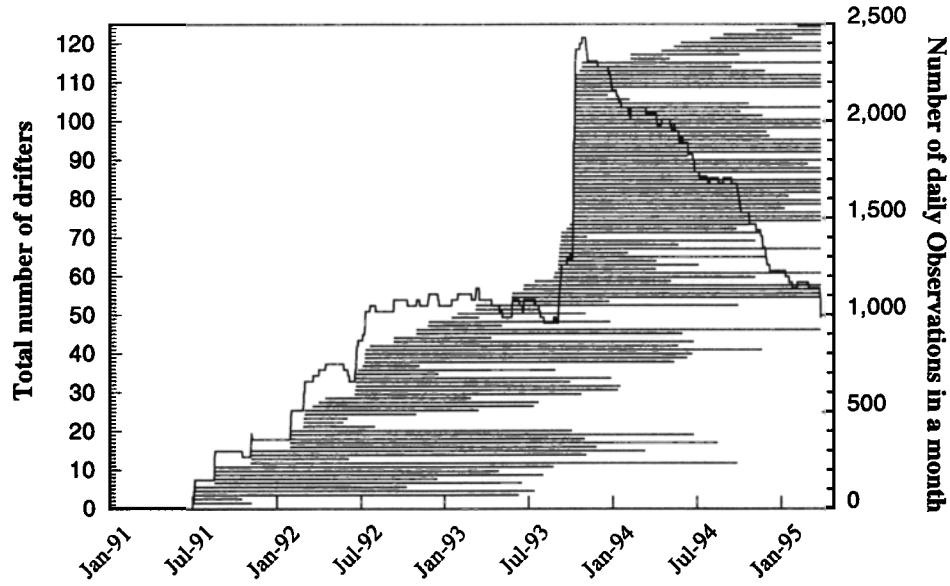

Figure 3. Time line and number of active drifters during January 1991 to April 1995. Each straight solid line indicates the working period of a drifter. The curved solid line indicates the number of daily observations in each month during that period.

due to mesoscale eddy activity and, possibly, due to secular changes on interannual timescales. The first of these limitations may be overcome through collection of many independent observations within a given subregion. It is not possible to reliably describe interannual variability or a seasonal cycle within this data set.

3.1. Lagrangian Correlations

The reliability of mean current estimates in the presence of mesoscale variability can be quantified by the standard error of the mean. At the 95% confidence level, this error of an east-west velocity component u is given by

$$u_{\text{error}} = \frac{1.96\sigma_u}{\sqrt{N^*}} \tag{1}$$

where σ_u is the measured standard deviation and N^* is the number of independent observations within a subregion [*Beyer*, 1987]. Similar equations hold for the north-south velocity component v and for the sea surface temperature. The estimate of N^* can be made by

$$N^* = \frac{N\Delta T}{\tau^L} \tag{2}$$

where N is the total number of observations, ΔT is the time interval between observations, and τ^L is a measure of the

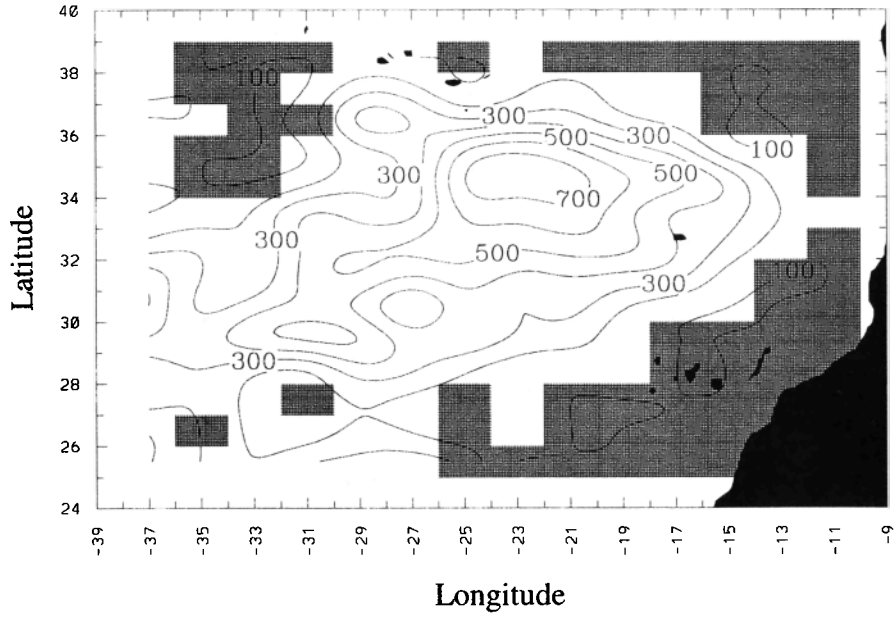

Figure 4. Number of daily observations in 1°×2° subregions. Areas where the number of daily observations is less than 100, or where the number of months represented in the average is less than 7, are shaded.

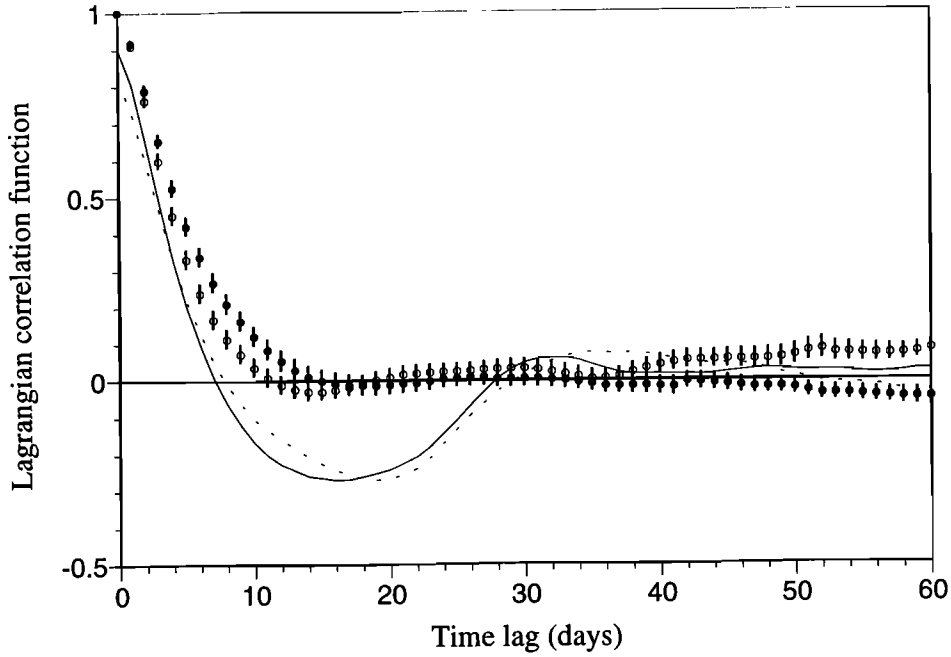

Figure 5. Lagrangian autocorrelation functions. The solid and open circles are the autocorrelation functions of u and v components, respectively. The vertical bars indicate the 95% confidence intervals. The dashed and solid lines represent the autocorrelation functions of u and v components of high-pass-filtered data, respectively. The window of the high-pass filter is equal to 50 days.

decorrelation time scale of a drifter motion, or twice the Lagrangian integral timescale [*Monin and Yaglom*, 1971]. The decorrelation time scale is estimated from the roll-off of the Lagrangian autocovariance function $R_{ij}(\tau)$ defined as

$$R_{ij}(\tau) = \frac{1}{T}\int_0^T u_i'(t)u_j'(t+\tau)dt \qquad i,j=1,2 \tag{3}$$

where u_i (i=1, 2) represents the u and v components of horizontal velocities, $u_i' = u_i - \langle u_i \rangle$ is the perturbation velocity, angle brackets are the ensemble average, τ is the time lag, and T is the length of the time series. Time-averaged velocities usually substitute the estimates of ensemble-averaged velocities. The calculation expressed in (3) has been outlined in several previous studies based on drifter data [e.g., *Poulain and Niiler*, 1989; *Paduan and Niiler*, 1993]. The Lagrangian autocovariance functions were calculated based on all the trajectories in the study area (Figure 5). If we assume that the mean current in the Canary Basin is approximately 0.1 cm s^{-1}, drifters could travel more than 400 km in 50 days. In such a timescale, drifters could flow eastward in the Azores Current and then recirculate westward in the countercurrents or the Canary Current. If we took the mean velocity of a drifter longer than 50 days, this recirculation pattern in the mean current field would represent a fluctuation. To eliminate such bias, we high-pass-filtered the drifter time series with a filter window of 50 days. The width of the filter window can be determined by trials. The high-pass-filtered data account for some 82% and 90% of the variance in the unfiltered u and v velocity components, respectively, when we took the filter window of 50 days. The Lagrangian autocorrelation functions based on all the trajectories within the study area are normalized by the zero-lag autocovariance $R_{ij}(0,T)$ of the unfiltered trajectories. The vertical bars indicate the 95% confidence intervals.

The Lagrangian integral time scale τ^L is determined by the integration of (3), the autocovariance functions [*Monin and Yaglom*, 1971]. *Inoue* [1950] and *Ogura* [1952] pointed out that $\tau^L < 2\tau^*$, where τ^* is satisfied by $R_{ij}(\tau^*)=0$, the zero crossings of the autocorrelation functions. The Lagrangian autocovariance functions of the high-pass-filtered data show τ^* approximately equal to 8 and 7 days for R_{uu} and R_{vv}, respectively. We use 16 days throughout this paper for the Lagrangian decorrelation timescale (or twice the Lagrangian integral timescale).

3.2. Eulerian Correlations

As the temporal decorrelation timescale of mesoscale variabilities can be investigated by the Lagrangian correlations, the spatial structure of mesoscale variabilities can be further studied by Eulerian longitudinal and transverse spatial covariances, R_L and R_T, defined as

$$R_L(\mathbf{x},t,\mathbf{r},\tau) = \left\langle \vec{v}_L'(\mathbf{x},t)\vec{v}_L'(\mathbf{x}+\mathbf{r},t+\tau)\right\rangle \tag{4}$$

$$R_T(\mathbf{x},t,\mathbf{r},\tau) = \left\langle \vec{v}_T'(\mathbf{x},t)\vec{v}_T'(\mathbf{x}+\mathbf{r},t+\tau)\right\rangle \tag{5}$$

where $\vec{v}_L'$ and $\vec{v}_T'$ are the longitudinal and transverse perturbation velocity components corresponding to the spatial lag $\mathbf{r}$ between two locations, and τ is the time lag between two measurements. Similar to the calculation of the Lagrangian correlations, we make the assumption that the mesoscale variability field is homogeneous and stationary, so that we have $R_L(\mathbf{x},t,\mathbf{r},\tau) = R_L(\mathbf{r},\tau)$ and $R_T(\mathbf{x},t,\mathbf{r},\tau) = R_T(\mathbf{r},\tau)$. In the calculation, we first binned the drifter data according to $\mathbf{r}$ and τ into boxes having the resolution of 40×40 km^2 in zonal and meridional directions, and 1 day in time. We removed the means of longitudinal and transversal components and then calculated and normalized Eulerian correlation functions

based on (4) and (5), using all the trajectories within the study area and the zero lag covariances R_L (0, 0) and R_T (0, 0) (Figure 6).

The spatial structure of mesoscale variabilities is anisotropic from the zero day lag Eulerian longitudinal and transverse correlation functions. The longitudinal correlation decreases faster in the SE-NW direction than it does in the NE-SW direction. We cannot determine the spatial scale from the first zero crossing of the longitudinal correlation because there is no obvious enclosed zero contour line. This can be biased by the homogeneous assumption because the current fields are nonhomogeneous in the Canary Basin. The transverse correlation is determined by rotational motion. Its spatial scale is a good indicator of the spatial scale of mesoscale eddy field. The spatial scale determined by the first zero crossing of the transverse correlation varies from 100 km in the SE-NW direction to 140 km in the NE-SW direction. Thus the time and spatial scales of an independent observation following a drifter path are equal to 7 to 8 days and 100 to 140 km, respectively.

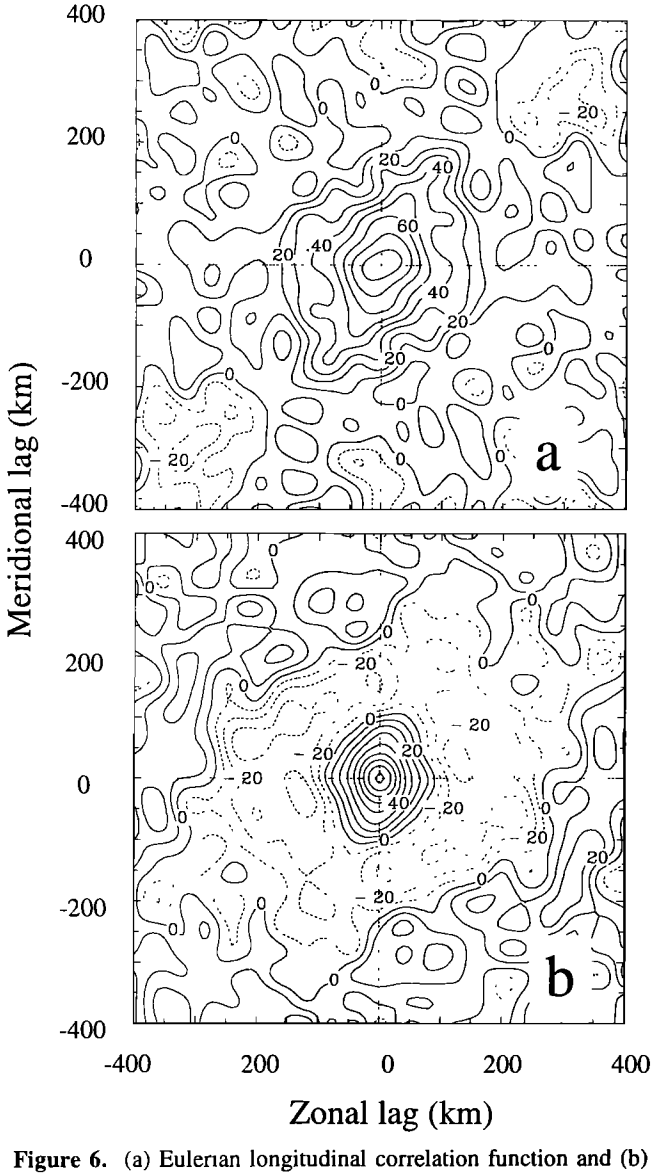

Figure 6. (a) Eulerian longitudinal correlation function and (b) Eulerian transversal correlation function. The contour interval is equal to 0.1.

3.3. Single Particle Diffusivity.

Statistical reliability of mean values determined from drifter observations is also limited by spatial variations in the data distribution. Mean current estimates can be systematically biased by uneven data distribution in the presence of eddy diffusivity. *Davis* [1991] referred to this effect as array bias, $\mathbf{u}_{bias}$ and defined it according to

$$\mathbf{u}_{bias} = -\kappa^{\infty} \cdot \nabla \ln(C) \tag{6}$$

where C is the drifter concentration and κ^{∞} is the eddy diffusivity tensor. The concentration gradients are visible in the spatial distribution of drifter data, and the maximum is at the center of the study area co-occurring with the sites of drifter deployments (Figure 4).

When estimating eddy diffusivity from drifter data, it is common to invoke homogeneous and stationary turbulence theory [*Taylor*, 1921] to relate κ^{∞} and $R_{ij}(t)$ [e.g., *Poulain and Niiler*, 1989; *Paduan and Niiler*, 1993; *Giannetti*, 1993]. Alternatively, the diffusivity may be estimated directly through the variation of Lagrangian properties of drifters passing through a given subregion as outlined by *Davis* [1991]:

$$\kappa_{ij}(\mathbf{x}, t) = \langle v_i'(t_0 \mid \mathbf{x}, t_0) d_j'(t_0 - t \mid \mathbf{x}, t_0) \rangle \quad i, j = 1, 2 \tag{7}$$

where v'_i and d'_j are departures from the Lagrangian mean velocity and displacement, respectively. The notation is such that $v_i(t|\mathbf{x}, t_0)$ is the value $v_i(t)$ of the particle passing through $\mathbf{x}$ at time t_0. An extensive discussion of (7) and the sensitivity of eddy diffusivity estimates in the California Current is given by *Swenson and Niiler* [1996]. In this study we apply the equation to drifter trajectories passing through 1° × 2° subregions. Furthermore, we approximate eddy diffusivity as

$$\kappa^{\infty}(x) = \kappa(x, t \to \infty) \approx \kappa(x, t \to \tau^{\infty}) \tag{8}$$

where we choose the Lagrangian integral timescale as τ^{∞} which is equal to 16 days. If the diffusivities are the integrals of corresponding covariances, these integrals should approach to constants when t is larger than τ^{L}. The residual difference of κ^{∞} between choosing τ^{∞} equal to 16 days and 30 days is less than 2%.

The principal diagonal elements of the diffusivity in the Canary Basin are presented in Figure 7. The diffusivity structure is generally zonal. The largest values are found along 34°N, which are associated with the Azores Current. Variable κ_{11} is approximately equal to 8×10^7 cm^2 s^{-1} in the vicinity of the current and decays to about one half that value within a few degrees north or south of 34°N. Throughout most of the domain, κ_{22} values are similar to κ_{11} but slightly weaker. The highest diffusivities in the northwest portion of the study area may be associated with the extension of the North Atlantic Current west of the Azores Islands, although the data density is relatively low in that region, which can bias the results. In general, the diffusivity values are consistent with the estimates obtained by *Giannetti* [1993], who applied the method developed by *Taylor* [1921] to the first half of the drifter data in this study obtained before May 1993.

The off-diagonal elements of the diffusivity tensor κ_{12} and κ_{21} presented in Figure 7, unlike the principal diagonal elements, do not exhibit spatial patterns that can be easily identified within features of the currents. The values of off-diagonal diffusivity elements range over $\pm1.5\times10^7$ cm^2 s^{-1}, and

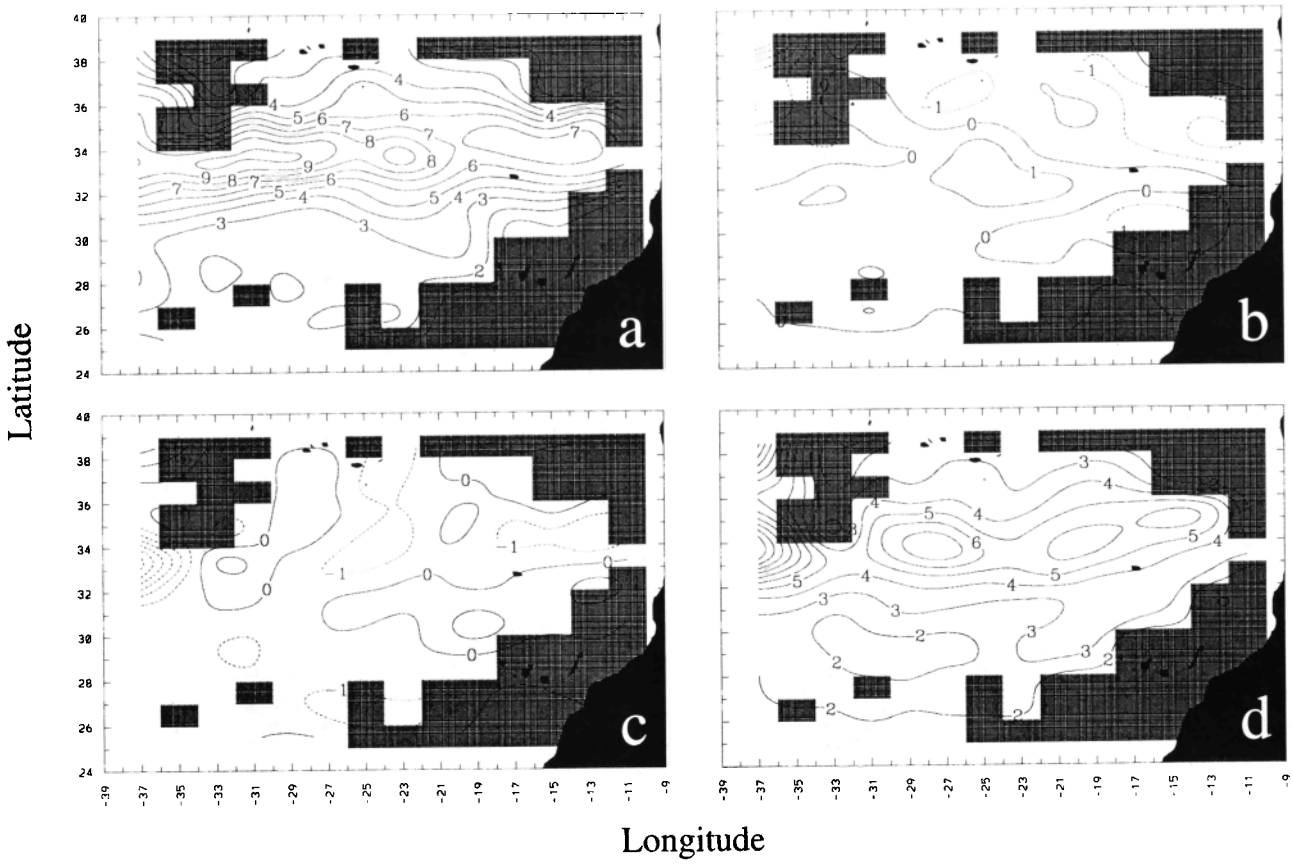

Figure 7. Eddy diffusivity tensor ($\times 10^7$ cm^2 s^{-1}): (a) κ_{11}, (b) κ_{12}, (c) κ_{21}, and (d) κ_{22}. The contour interval is equal to 1 ($\times 10^7$ cm^2 s^{-1}).

their absolute values are typically 5 times smaller than the colocated principal diagonal elements.

3.4. Mean Currents and Variability

The multiyear-averaged surface currents in 1°×2° subregions of the Canary Basin are presented in this section together with different measures of the uncertainty of means. In all cases, mean current vectors have been corrected for array biases using the following formula [*Davis*, 1991]:

$$\langle \mathbf{u} \rangle = \frac{\int_{\mathbf{A}} \left[\mathbf{u}(\mathbf{x}) C(\mathbf{x}) + \kappa^{\infty}(\mathbf{x}) \cdot \nabla C(\mathbf{x}) \right] d\mathbf{A}}{\int_{\mathbf{A}} C(\mathbf{x}) d\mathbf{A}} \tag{9}$$

where $\mathbf{u}$ is the drift velocity, $\langle \mathbf{u} \rangle$ is the bias-corrected mean velocity, and $\mathbf{A}$ represents the area of a 1°×2° subregion. This corrected velocity is a concentration-weighted ensemble average minus an apparent velocity due to the down-gradient diffusion of drifters. In most parts of the study area the array bias equation (6) represents a small correction to the mean velocity. Array bias correction vectors ($-\mathbf{u}_{bias}$) are shown in Figure 8 for a comparison with the drifter concentration map (Figure 4). The correction vectors are directed toward the concentration maxima. The maximum biases have magnitudes of approximately 6 cm s^{-1}, but most of the magnitudes are less than 2 cm s^{-1}.

Bias-corrected mean current vectors are shown in Figure 8b together with 95% confidence error ellipses equation (1). In the figure, vectors from areas with less than 100 drifter days of observations are not shown. In addition, to avoid the seasonal bias, any areas with observations in less than seven different months represented in the average are also eliminated. Mean vectors are significantly larger than their errors over most of the study area, particularly where mean currents are strongest.

The variability of currents in each subregion can be studied by the eddy kinetic energy (EKE) EKE=½($\langle u'^2 \rangle$+$\langle v'^2 \rangle$) constructed from u' and v' (Figure 9). Results simply indicate that variations of currents in subregions are larger than mean currents, and therefore it is necessary to repeatedly sample a given region to extract the mean. This is precisely why this study was designed around repeated deployments of drifters over multiple years.

4. Sea Level

We can further calculate the sea levels by using the momentum equations in the Ekman layer, that is,

$$\left\langle \frac{d\mathbf{u}}{dt} \right\rangle + f\,\hat{\mathbf{k}} \times \langle \mathbf{u} \rangle = -g \nabla \langle \zeta \rangle + \frac{\partial \langle \tau \rangle}{\partial z} \tag{10}$$

where $d(\cdot)/dt = \partial(\cdot)/\partial t + u\partial(\cdot)/\partial x + v\partial(\cdot)/\partial y$, f is the Coriolis parameter, $\hat{\mathbf{k}}$ is the unit vector normal to the Earth's surface, ζ is the sea level, and τ is the vertical shear stress. In (10) we have neglected $\langle w \partial \mathbf{u}/\partial z \rangle$, where w is the vertical velocity component since the first-order balance for meso-scale and large-scale motion is geostrophic or Ekman [*Pedlosky*, 1987].

We first use drifter data to estimate $\langle d\mathbf{u}/dt \rangle$ and $\langle \mathbf{u} \rangle$. Then, to investigate the vertical gradient of shear stress, we obtained

the multiyear operational wind products for our study region from the European Centre for Medium-Range Weather Forecasts (ECMWF) [*Simmon and Dent*, 1989] and employed the formula of wind-driven velocities developed by *Pollard and Millard* [1970] and *Ralph and Niiler* [1999]. The mean wind vectors in 1°×2° bins from that data set are shown in Figure 10. Following *Ralph and Niiler* [1999], the wind-driven current can be written as

$$\mathbf{u}_a = \beta f^{-1/2}\mathbf{u}_* e^{-i\theta} \tag{11}$$

where $\mathbf{u}_a$ and $\mathbf{u}_*$ are the complex expressions of ageostrophic current velocities and the friction velocity of surface stresses, respectively, and θ is the direction of the current. In (11), β and θ are constants to be determined from observations. From the Ekman balance, the vertical gradient of shear stress can then be expressed as

$$\frac{\partial \tau}{\partial z} = \beta f^{1/2} u_* e^{i(\theta_w - \theta + \pi/2)} \tag{12}$$

where θ_w is the direction of wind. The uniqueness of sea level at a given location requires the line integral of the sea level gradient along any closed curve be equal to 0. Because of errors within the measurements, this condition is hard to meet, which leads to a residual error ε_i in each 1°×2° subregion defined by an enclosed curve C_i, that is,

$$\varepsilon_i = \oint_{c_i}\left[\left\langle\frac{d\mathbf{u}}{dt}\right\rangle + \mathbf{f}\times\langle\mathbf{u}\rangle - \frac{\partial\langle\tau\rangle}{\partial z}\right]\cdot d\mathbf{r} \tag{13}$$

where $\mathbf{r}$ is the tangent to curve C_i. We define the least squares error ε^2 of our study region as

$$\varepsilon^2 = \frac{1}{N_b}\sum_i\left\{\oint_{c_i}\left[\left\langle\frac{d\mathbf{u}}{dt}\right\rangle + \mathbf{f}\times\langle\mathbf{u}\rangle - \frac{\partial\langle\tau\rangle}{\partial z}\right]\cdot d\mathbf{r}\right\}^2 \tag{14}$$

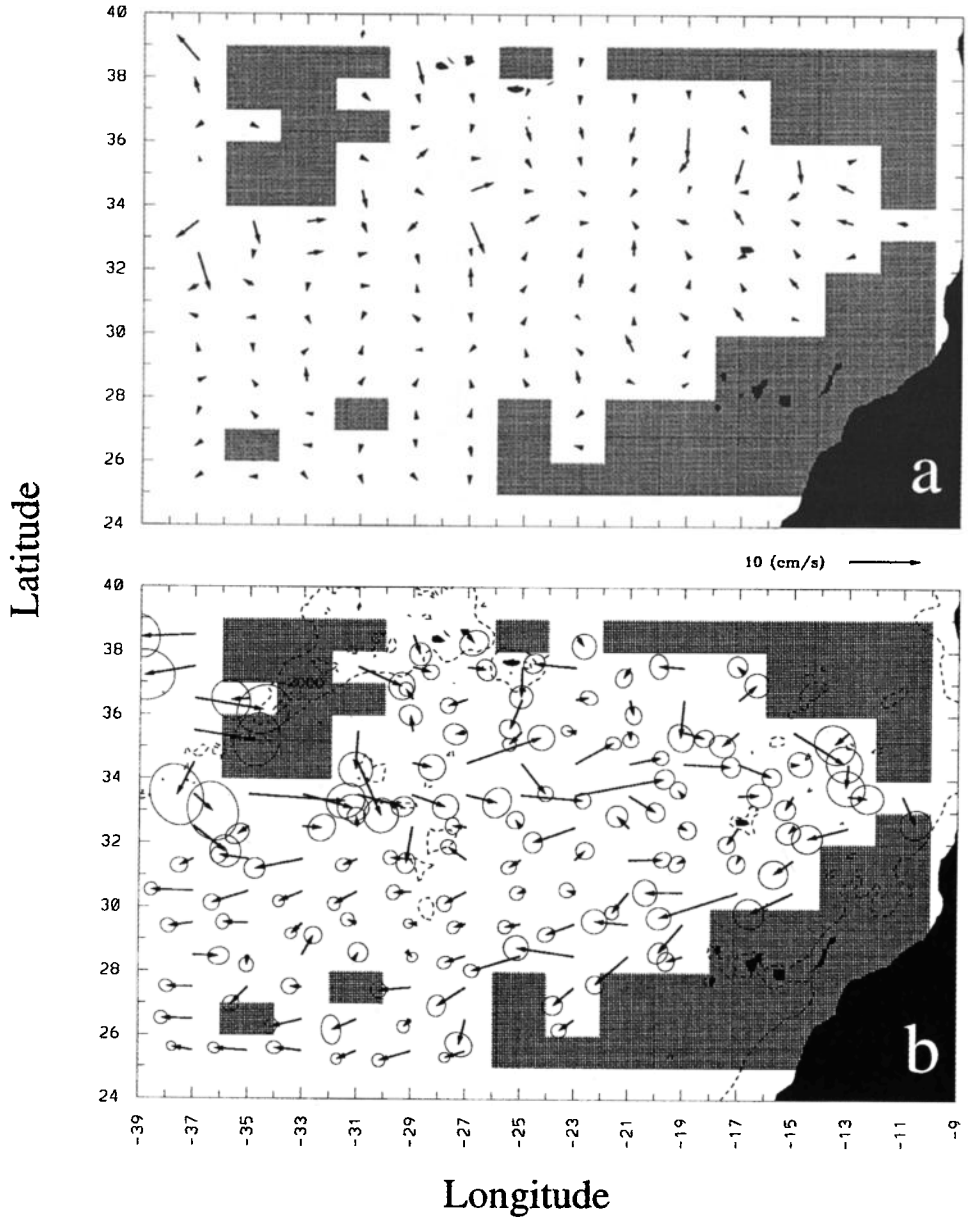

Figure 8. (a) The array bias correction vectors and (b) the mean surface currents from drifter observations (vectors) and associated 95% confidence error ellipses.

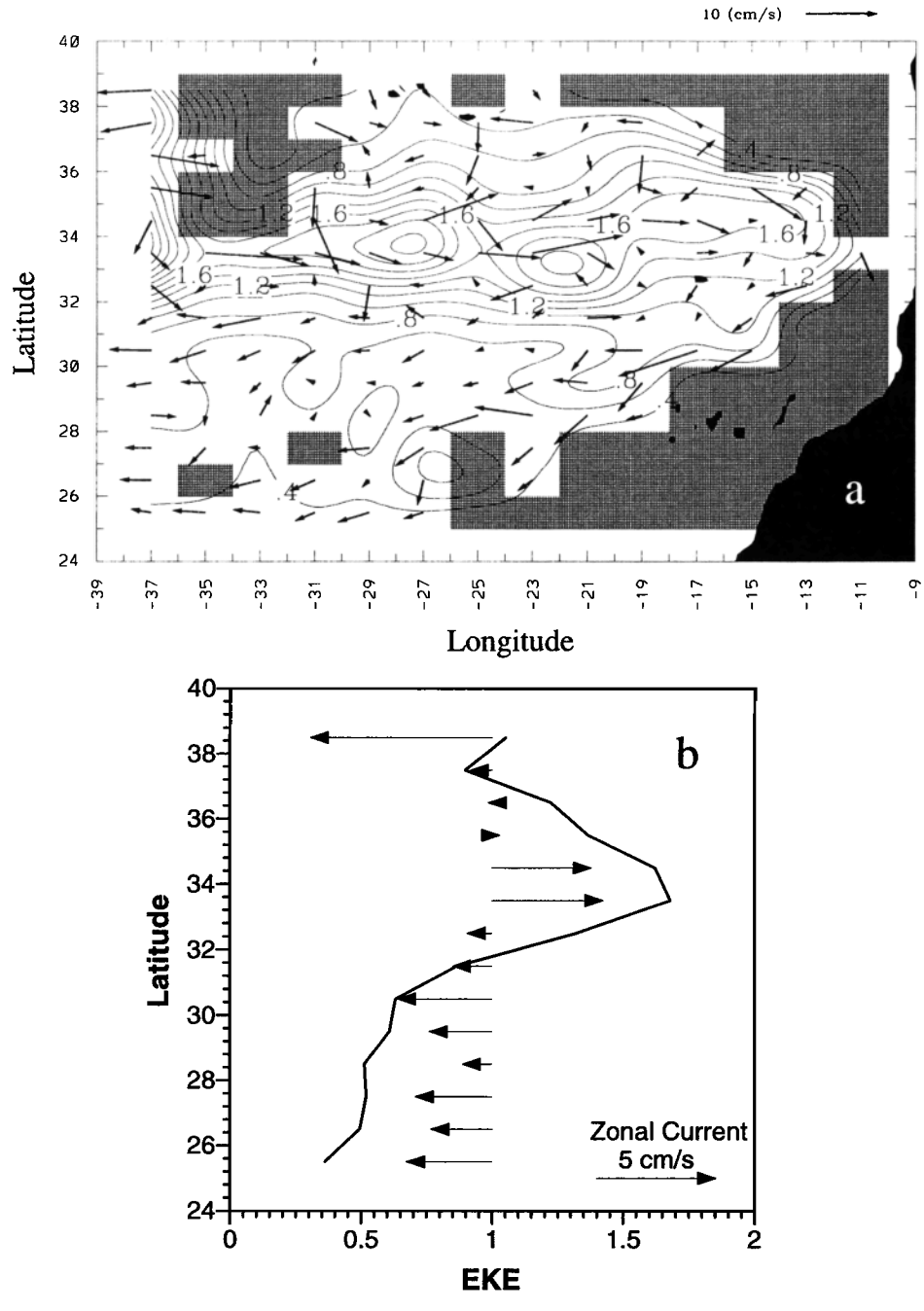

Figure 9. (a) The mean surface currents from drifter observations (vectors) and contours of the associated eddy kinetic energy ($\times 10^2$ cm^2 s^{-2}) and (b) the zonally averaged zonal currents (vectors) and eddy kinetic energy ($\times 10^2$ cm^2 s^{-2}). The contour interval is equal to 0.2 ($\times 10^2$ cm^2 s^{-2}).

where N_b is the number of our subregions. Thus this least squares error is calculated from the sum of integrals over all enclosed curves C_i of 1°×2° subregions. By minimizing the least squares error, we have β and θ equal to 0.02 and 52.7°, respectively. The corresponding wind-driven velocities are shown in Figure 10a.

Absolute sea level can be determined by integrating (10), starting from a given sea level reference. Relative sea level, the departure from the mean, can be estimated by removing a grand mean in our study area (Figure 10b). The highest gradients of sea level are associated with the eastward Azores Current and the southwestward Canary Current along the continental slope.

5. Kinetic Energy Transfer and Mass Convergence

Beyond the mean current, eddy kinetic energy, and eddy diffusivity maps obtained from the drifter data, we further investigated the mechanical energy balances which provide insight into the dynamic processes of the creation and distribution of eddies produced by horizontal shear of mean currents.

5.1. Kinetic Energy Exchange

The Lagrangian nature of drifter data allows us to estimate $d(\cdot)/dt$ of any drifter measuring variable and to compute

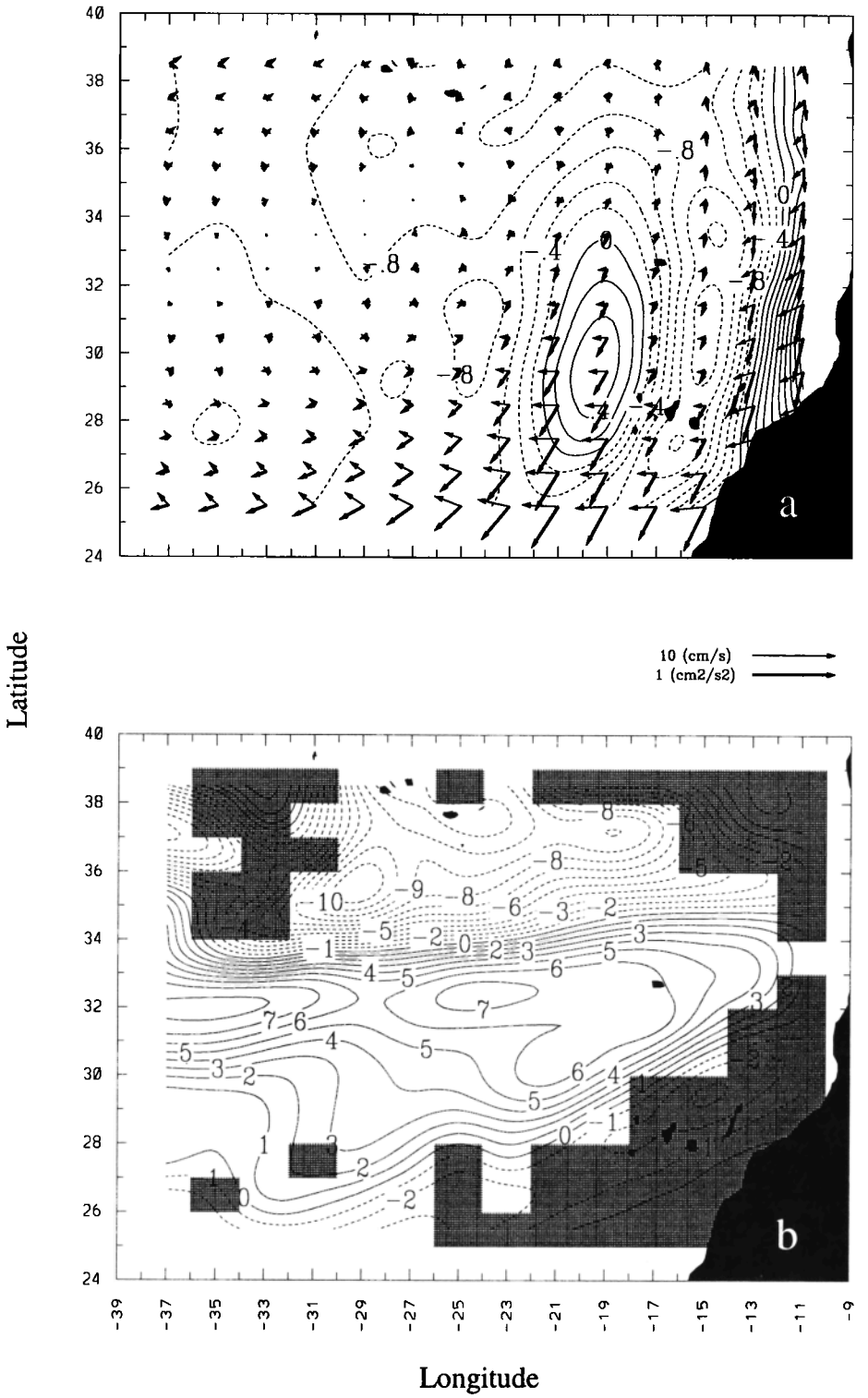

Figure 10. (a) Mean ECMWF wind stress (thicker vectors), wind-driven velocities (thinner vectors), and divergence ($\times 10^{-8}$ s^{-1}) driven by curl of the wind stress, and (b) the sea level anomaly (cm). The contour intervals for curl of the wind stress and the sea level anomaly are equal to 0.2 ($\times 10^{-8}$ s^{-1}) and 1 (cm), respectively.

Eulerian ensemble averages from multiyear observations in a subregion. The difference between the mean rate of change in kinetic energy of a water parcel in the surface layer and the rate of change in mean kinetic energy leads to the eddy kinetic energy equation, that is,

$$\frac{d(\mathrm{EKE})}{dt} = \left\{\left\langle \mathbf{u}\cdot\frac{d\mathbf{u}}{dt}\right\rangle - \langle\mathbf{u}\rangle\cdot\left\langle\frac{d\mathbf{u}}{dt}\right\rangle\right\} - \left\{\frac{\partial\left\langle\frac{1}{2}(u'^2+v'^2)u'\right\rangle}{\partial x} + \frac{\partial\left\langle\frac{1}{2}(u'^2+v'^2)v'\right\rangle}{\partial y}\right\} - \left\{\frac{\partial\left\langle\frac{1}{2}(u'^2+v'^2)u'\right\rangle}{\partial x} + \frac{\partial\left\langle\frac{1}{2}(u'^2+v'^2)v'\right\rangle}{\partial y}\right\} - \left\langle\frac{1}{2}(u'^2+v'^2)\frac{\partial w'}{\partial z}\right\rangle \quad (15)$$

The estimates of the first three bracketed terms on the right are shown in Figure 11. The first term on the right can be rewritten as

$$\left\langle \mathbf{u}\cdot\frac{d\mathbf{u}}{dt}\right\rangle - \langle\mathbf{u}\rangle\cdot\left\langle\frac{d\mathbf{u}}{dt}\right\rangle = \left\langle(\mathbf{u}-\langle\mathbf{u}\rangle)\cdot\left(\frac{d\mathbf{u}}{dt}-\left\langle\frac{d\mathbf{u}}{dt}\right\rangle\right)\right\rangle \quad (16)$$

which represents the work done on the fluctuation of horizontal velocities. Substituting (10) into (16), the right side can be further rewritten as $\langle -g\mathbf{u}'\cdot\nabla\zeta' - \mathbf{u}'\cdot\partial\tau'/\partial z\rangle$. If the fluctuation of velocities has only both Ekman and geostrophic components associated with wind fluctuation and quasigeostrophic mesoscale features, in the first term, the dot product between geostrophic components and sea level gradients is 0. In the second term, because the mean gradient of the vertical shear stress is 90° off relative to the wind driven ageostrophic current (12), the product of these two components is equal to 0. In the remaining terms, the dot products between the wind-driven velocities and mesoscale sea level fluctuation, and between geostrophic balanced velocity fluctuation and wind stress, cancel each other. Thus (16) represents the EKE production done by the surface slope and wind stress over velocity which are not under geostrophic and Ekman balances. The work is positive in most of our study area in the Canary Basin. Negative values are found in the region of the eastern extension of the Azores Current, northwest of Madeira Island, and within the Canary Current along the continental shelf.

The second term is the work done by Reynolds stress on mean flow, within which contributions from vertical velocity fluctuations are not included because drifters measure only horizontal velocity components. The maximum of energy transfer (6×10^{-5}cm^2 s^{-3}) from the mean Azores Current to random kinetic energy occurs at 34°N, 28°W. Within the eastern extension of the Azores Current, Reynolds stress plays the opposite role, which transfers the energy from random motion to the mean currents.

The third term is the third-order correlations of velocity fluctuations, representing the dispersion fluxes of eddy kinetic energy produced by eddy motion itself, which can be calculated directly from drifter data. Similar to the work done by Reynolds stress, a positive maximum is found at 34°N, 28°W, and negative maxima are within the eastern extension of the Azores Current. Apparently, it is not the case that eddy kinetic energy is dispersed simply from maxima to minima by eddy motion, by which positive regions should be found around the EKE maxima, and on both sides of the Azores Current.

The last term on the right represents the change of EKE produced by stretching of the water column due to eddy motion. Because drifters only measure horizontal motion, it is prohibited to compute this term directly. Noticing the results from Eulerian spatial correlation functions that the mesoscale eddy field has a spatial scale of 100-140 km, the flow within an eddy is quasigeostrophically balanced [*Rudnick and Luyten*, 1996]. Consequently, $\|w'\|/\|z\|$ is at least 1 order of magnitude smaller than $\|u'\|/\|x\|$, where $\|u'\|$ and

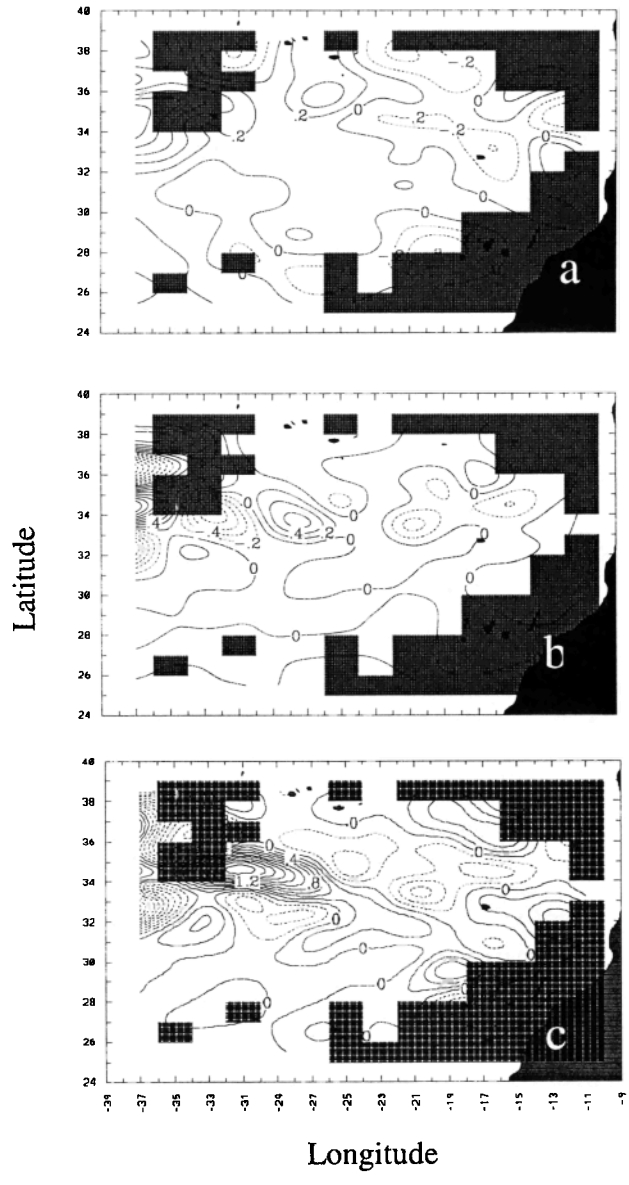

Figure 11. (a) The work done by external forces on eddy currents, $\langle\mathbf{u}\cdot d\mathbf{u}/dt\rangle - \langle\mathbf{u}\rangle\cdot\langle d\mathbf{u}/dt\rangle$ ($\times10^{-4}$ cm^2 s^{-3}), (b) the work done by Reynolds stress on mean currents, $\langle u'_i u'_j\rangle\cdot\langle u_i\rangle_{,j}$ ($\times10^{-4}$ cm^2 s^3), and (c) the dispersion of EKE by eddy motion, $-\langle\frac{1}{2}(u'_1{}^2+u'_2{}^2)u'_i\rangle_{,i}$ ($\times10^{-4}$ cm^2 s^{-3}). The contour interval is equal to 0.2 ($\times10^{-4}$ cm^2 s^{-3}).

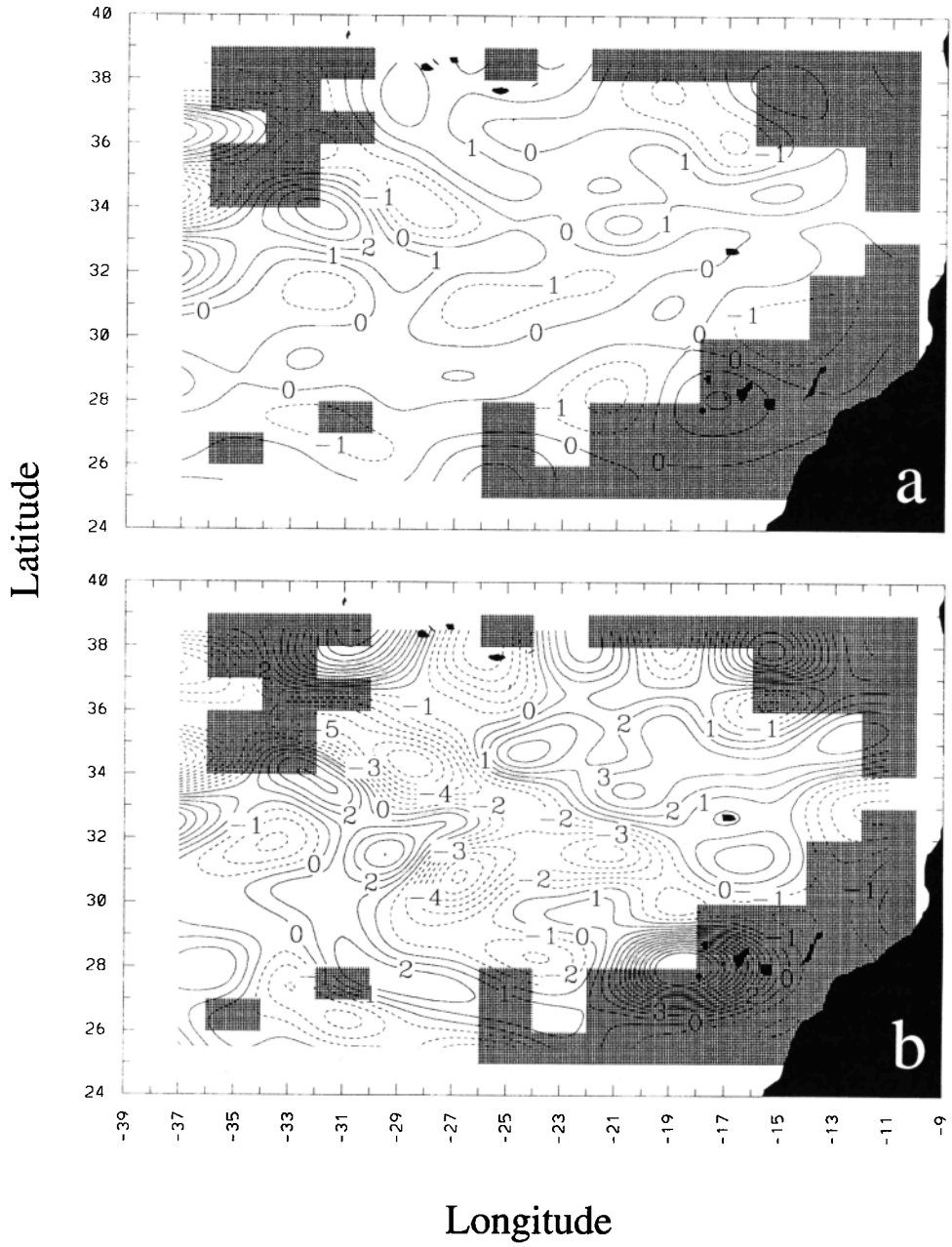

Figure 12. (a) The convergence computed directly from drifter velocities ($\times 10^{-7} s^{-1}$) and (b) the convergence computed from the kinetic energy balance ($\times 10^{-7} s^{-1}$). The contour interval is equal to 0.1 ($\times 10^{-7} s^{-1}$).

$\|w'\|$ are the horizontal and vertical velocity scales of an eddy, and $\|x\|$ and $\|z\|$ are the horizontal and vertical length scales, respectively. Thus this term is negligible.

5.2. Convergence

The difference between $\langle u'u' \rangle$ and $\langle v'v' \rangle$ is estimated by the ratio of $2\times(\langle u'u' \rangle - \langle v'v' \rangle)$ to $(\langle u'u' \rangle + \langle v'v' \rangle)$. The mean of this ratio is equal to 0.10 with the standard deviation of 0.076 and 95% confidence of 0.013. The isotropy of Reynolds stress can be evaluated by the ratio of $(2\times\langle u'v' \rangle)$ to $(\langle u'u' \rangle + \langle v'v' \rangle)$. In the Canary Basin the mean of this ratio is equal to 0.11 with the standard deviation of 0.083 and 95% confidence of 0.014. The computed off-diagonal components of Reynolds stress are 1 order of magnitude smaller than the diagonal components. Hence Reynolds stress is nearly isotropic. The work done by Reynolds stress can be further expressed as

$$\begin{aligned} &\langle u'u' \rangle \frac{\partial \langle u \rangle}{\partial x} + \langle u'v' \rangle \frac{\partial \langle u \rangle}{\partial y} + \langle v'u' \rangle \frac{\partial \langle v \rangle}{\partial x} + \langle v'v' \rangle \frac{\partial \langle v \rangle}{\partial y} \\ &\approx \langle u'u' \rangle \frac{\partial \langle u \rangle}{\partial x} + \langle v'v' \rangle \frac{\partial \langle v \rangle}{\partial y} \\ &\approx \langle u'u' \rangle \nabla \cdot \langle \mathbf{u} \rangle \end{aligned} \tag{17}$$

Hence substituting the approximation of (17) into expanded (15), the work done by Reynolds stress can provide an independent estimate of the convergence when scaled by the variance $\langle u'u' \rangle$, that is,

$$-\nabla\cdot\langle\mathbf{u}\rangle \approx -\left\{\left\langle \mathbf{u}\cdot\frac{d\mathbf{u}}{dt}\right\rangle - \langle\mathbf{u}\rangle\cdot\left\langle\frac{d\mathbf{u}}{dt}\right\rangle - \langle\mathbf{u}\rangle\cdot\nabla\left\langle\frac{1}{2}|\mathbf{u}'|^2\right\rangle - \nabla\cdot\left\langle\frac{1}{2}|\mathbf{u}'|^2\mathbf{u}'\right\rangle\right\}\Big/\langle u'u'\rangle \quad (18)$$

The convergence so estimated is shown in Figure 12b, together with the direct computation from the bias-corrected mean current field (Figure 12a). The two estimates are significantly correlated, which lends confidence to the patterns observed for the traditionally hard to obtain convergence of mean currents. The regression between the two convergence estimates in Figure 12 is shown in Figure 13. The correlation coefficient r^2=0.56 and the best fit slope is 0.55, indicating that the magnitude of convergence computed from the EKE budget exceeds that computed kinematically in most places.

The error in the directly computed convergence can be simply estimated by the sum of the variances of all terms if the measurements are independent in respect to both locations and directions. From the above analysis that the standard deviations in x and y directions are nearly same, the standard deviation is equal to 2 time the standard deviation of the mean currents divided by Δx or Δy. Thus, if the relative error of the mean current at 95% confidence varies from 10 to 20%, we expect that the relative error of the estimated convergence should be approximately from 20 to 40%.

6. Heat Transports

Further dynamic insights will be gained by investigating the heat balance in the subduction region from the multiyear drifter observations of sea surface temperature. In order to quality control the drifter temperature data, we generated another drifter temperature data set along drifter trajectories from 1°×1° weekly sea surface temperature maps produced by National Center for Environmental Prediction (NCEP) at NOAA [*Reynolds and Smith*, 1994]. These two data sets are exactly the same. Our temperature distribution agrees with the sea surface temperature distribution based on climatological data assessed by *Bunker* [1976] and *Reynolds and Smith* [1995]. The mean temperature within the resolution of 1°×2° shows a smooth southwestward gradient (Figure 14). The temperature increases from 18°C at 39°N, 17°W to 24°C at 25°N, 36°W. The contour lines are curved southward west of the Madeira and Canary Islands, which elucidates the advection effects of the Canary Current and the upwelling along the African coast.

The estimates of mean Eulerian currents and mean Ekman layer temperature allow us to further calculate the meridional temperature fluxes (QH) in the Canary Basin, which is defined as

$$Q_H = \int_{37°W}^{9°W}\int_{-H}^{0} \rho\, c_p \langle T\rangle\langle v\rangle dz dx \quad (19)$$

where ρ is the surface water density, cp is the specific heat capacity of seawater, QH is the meridional temperature fluxes in the Ekman layer integrated from 37°W to the east limit of our drifter observations near the African and European coast, and H is the Ekman layer depth. An average Ekman layer depth of 50 m is assumed [*Stramma and Isemer*, 1988]. This

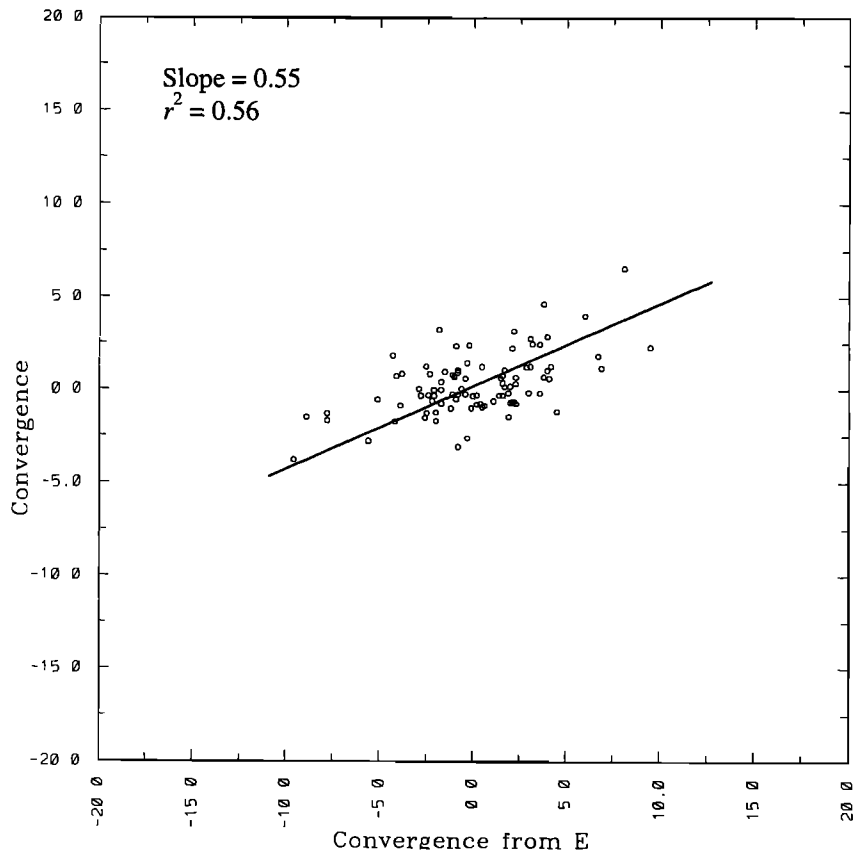

Figure 13. The scatter diagram between two different convergence estimates (×$10^{-7}s^{-1}$) in Figure 12. Round circles are the estimates in Figure 12, and the solid line is the regression relation between these two convergence estimates.

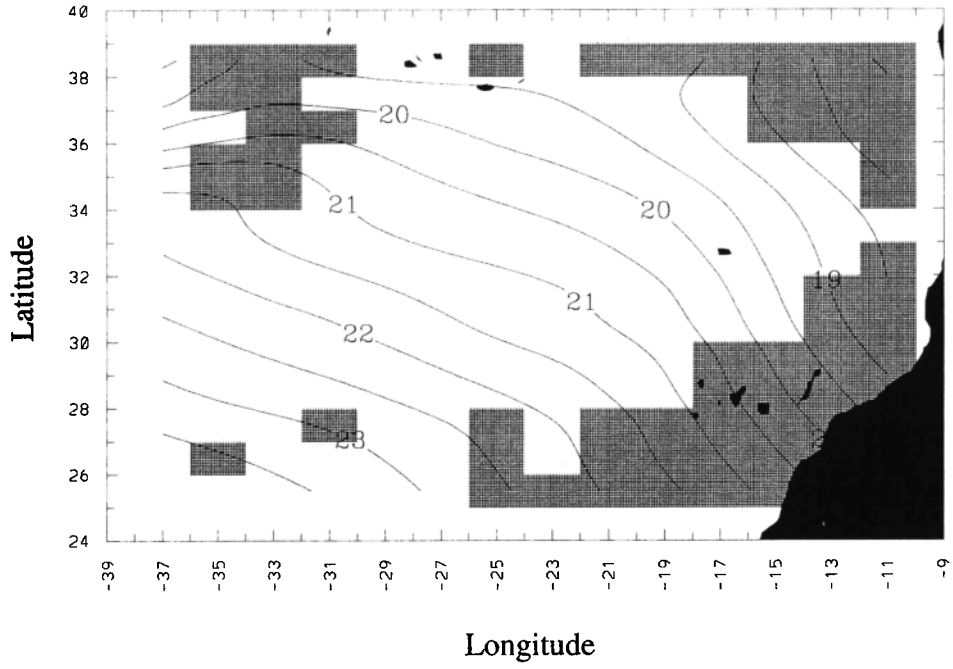

Figure 14. Mean sea surface temperature (°C) from drifter measurements. The contour interval is equal to 0.5 (°C).

integrated meridional temperature flux is presented in Figure 15 as a function of latitude between 25°N and 39°N. The estimates are scattered between -0.17~-0.03×10^{15} W. The mean of the temperature flux is equal to -0.076×10^{15} W with a standard variation of 0.022×10^{15} W, which demonstrates a mean southward cool water advection.

To understand the local surface heat fluxes and heat balance, we assume that the temperature in the Ekman layer is nearly uniform, so that the heat balance can be written as

$$\rho c_p \frac{dT}{dt} = \frac{Q_s - Q_b}{H} \tag{20}$$

where Q_s and Q_b are vertical turbulent heat fluxes through the surface and bottom of an Ekman layer, respectively. We could directly calculate the heating rate of the surface Ekman layer in a subregion, that is, $\rho c_p \langle dT/dt \rangle$. However, such calculations can be easily biased by the uneven distribution of drifter data in different seasons. To avoid this bias, we first remove the seasonal trend of temperature from the drifter data based on the 1°×1° weekly sea surface temperature estimated by NCEP. Then we further explore the heat balance by expanding $\langle dT/dt \rangle$, that is,

$$\left[\left\langle \frac{dT}{dt} \right\rangle - \left\langle \frac{\partial T}{\partial t} \right\rangle\right] = \left[\langle u \rangle \frac{\partial \langle T \rangle}{\partial x} + \langle v \rangle \frac{\partial \langle T \rangle}{\partial y}\right] + \left[\frac{\partial \langle u'T' \rangle}{\partial x} + \frac{\partial \langle v'T' \rangle}{\partial y}\right] + \left\langle T' \frac{\partial w'}{\partial z} \right\rangle \tag{21}$$

where we removed the ensemble mean of local changes of temperature $\langle \partial T/\partial t \rangle$ from $\langle dT/dt \rangle$ to further correct our limited number of observations. The term on the left side of (21) is the anomaly of surface heating from the seasonal heating and cooling. On the right side, the first term is the mean flow advection, and the second term is horizontal heat diffusion due to fluctuations of horizontal currents and temperature. These two terms can be directly calculated from the binned drifter data. Figure 16 shows the estimates of the term on the left side of (21), and the first two terms on the right side. The results show that the horizontal heat advection and diffusion have the same order of magnitude as the anomaly of surface heating.

7. Discussion

7.1. Mean Flow Fields

The psuedo-Lagrangian nature of drifter observations makes it possible to estimate horizontal diffusivity. The numerical values of the principal diagonal components κ_{11} and κ_{22} range between 3×10^7 cm^2 s^{-1} and 8×10^7 cm^2 s^{-1}. The largest diffusivity is associated with the strongest flow in the Azores Current. Different from the principal diagonal elements, the off-diagonal elements of the diffusivity κ_{12} and κ_{21} do not exhibit spatial patterns that can be easily identified with features in the currents. The values of the off-diagonal diffusivity elements range over ±1.5×10^7 cm^2 s^{-1}, and their absolute values are typically 5 times smaller than the colocated diagonal elements.

The estimates of horizontal diffusivity permit us to employ the formula developed by *Davis* [1991] to remove the array bias from mean currents. In most parts of the study area the array bias represents a small correction to the mean velocity. Because drifters can be concentrated by the convergent flow, which leads to high array bias, this correction is critical to estimate the convergence field. If we take the principle axis of the Azores Current from 33.5°N at 35°W, to 34°N at 18°W, the convergence map computed kinematically based on

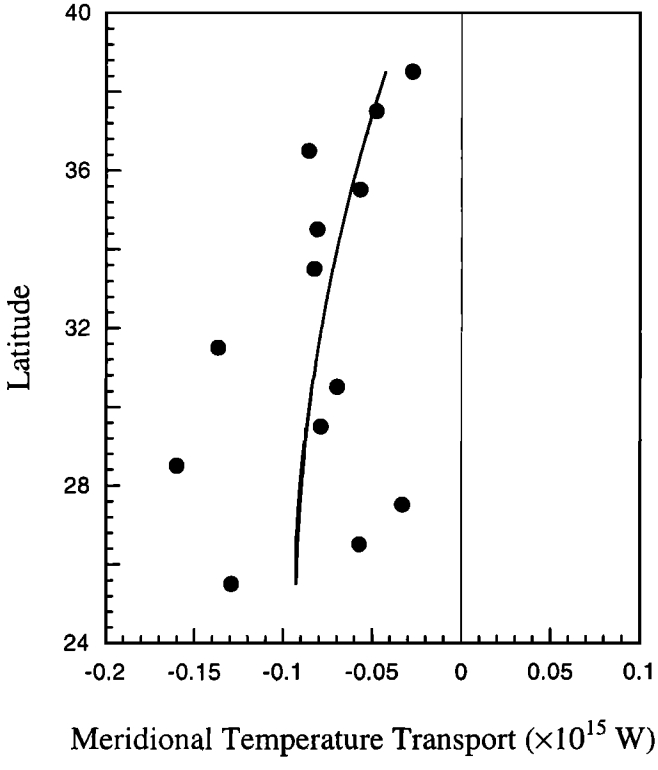

Figure 15. Meridional temperature flux (1015 W) within the surface mixed layer (0-50 m depth) in the eastern North Atlantic Ocean between 37°W and the African and European coast. Solid circles are the estimates from drifter data. The solid line is the regression of a second-order polynomial function (r^2=0.24).

the corrected mean currents revealed two regions of maximum convergence. One is centered at 33.5°N, 32°W, where the Azores Current decelerated and is joined with a southward current. East of this convergence there is a tongue of divergence extending from the northwest to the southeast, associated with two small branches spinning off from the mean current. Further east, the convergence follows the Azores Current. The contour line of 1×10^{-7} s^{-1} indicates that the convergence is relatively higher north of the Azores Current than that south of the current. Utilizing the nearly isotropic nature of Reynolds stress and the eddy kinetic energy balance equation in this study area, we further derived this convergence pattern from the turbulent energy equation.

The convergence estimated from the wind stress curl is 10^{-8} s^{-1}, 1 order of magnitude smaller than the convergence estimated from the mean currents (Figures 10a and 12). Both also show different convergent patterns. The wind stress curl shows a convergence centered at 29.5°N, 19.5°W. Thus other processes instead of wind stress curl produce the convergence estimated from drifter data. All terms in the denominator on the right side of (18) are of the same order. The first term, the correlation between the fluctuation of wind stresses and horizontal velocities indicated in the previous discussion, dominates the convergence in the east extension of the Azores Current (Figure 11). The second term is relatively small. The third term, the dispersion of EKE, dominates the divergence south of the Azores Islands.

Our convergence estimates are associated with the mean flow field at a spatial scale of 200 km determined by the scale of subregions. Assuming the Ekman layer depth of 50 m, the maximum downwelling velocity is approximately equal to 1 m d^{-1}. It is obvious from (18) and the above discussions that the convergence of mean current is produced by mesoscale eddy fields. *Rudnick* [1996] used the ω equation, quasigeostrophic method of *Hoskins et al.* [1978] to estimate vertical downwelling velocities in the mixed layer. His results showed that downwelling reaches approximately 7 m d^{-1} along the northern side of the front. The horizontal extent of downwelling patches observed was small at approximately 10 km. However, the convergence computed from quasigeostrophic balance is only a portion of the total convergence. Equation (18) indicates that the correlation between fluctuations of wind stresses and currents is of the same order of other terms. Our estimated convergence field is the average of these 10 km downwelling features over 200 km subregions.

Many important features of the surface circulation of the Canary Basin are evident in Figure 9. The current system associated with the subtropical convergence zone in this area (the Azores Current) is clearly visible in the mean currents around 34°N. Mean speeds within the Azores Current system are typically 10-15 cm s^{-1} The Azores Current bifurcates around 22°W, with the major branch of the current continuing eastward, circles the Madeira Plateau around 32.5°N, 17°W, and then joins the Canary Current along the continental slope between the Madeira Plateau and the Canary Islands. The Canary Current flows southwestward at the speed of 10-15 cm s^{-1}.

Both the Azores Current and the Azores front have a spatial scale from 50 to 100 km [*Gould*, 1985; *Käse et al.*, 1985; *Rudnick*, 1996]. The front is meandering and embedded in mesoscale eddies. The movement and meandering of the Azores Current leads to high variation in currents and high EKE (Figure 9) within the front region. Our drifter observation of the Azores Current represents the mean between July 1991 and January 1995. The location of the Azores Current observed by drifters is more confined within 33°N and 35°N compared to the climatological location of the Azores front between 32°N and 36°N [*Gould*, 1985; *Krauss and Käse*, 1984; *Spall*, 1990; *Stramma and Müller*, 1989]. This difference can be a result of (1) higher spatial resolution and higher density of drifter data, (2) a short observation period relative to a climatological timescale, and surface mixed layer current observed only by our surface drifters. However, the center of the Azores Current is located at 34°N consistent with the climatological center [*Gould*, 1985; *Stramma and Isemer*, 1988].

The historic data shows that the Azores Current is a strong flow of approximately 10 Sv [*Gould*, 1985; *Stramma and Isemer*, 1988]. If we take the mean surface Azores Current of 10 cm s^{-1}, the Ekman layer depth of 50 m and the (latitudinal) mean width of 200 km, the volume flux of the surface Azores Current is approximately 1 Sv, or 10% of the total volume flux. The Azores Current has to penetrate into a great depth that has been observed.

North and south of the Azores Current, evidence is seen for westward flowing countercurrents. Strong evidence of a countercurrent north of the Azores Current was shown recently by *Cromwell et al.* [1996] based on hydrography and repeated altimetry crossings near 28°W. They found persistent westward flow between 34°N and 36°N during two separate 3-month periods in 1992 and 1994, which they attributed to recirculation of the main Azores Current. Our

observations provide the alternate possibility that the countercurrent is fed by the strong southward flow at 25°W observed to originate just south of the Azores Islands. Between the Azores Current and countercurrents, there exist rich mesoscale eddies [*Käse et al.*, 1986; *Käse and Siedler*, 1982; *Käse et al.*, 1985; *Rudnick*, 1996].

North of the Azores Current between the Azores Islands and Portugal, there is a broad weak southward current, called the Portugal Current [*Saunders*, 1982; *Sverdrup* et al., 1942]. Our drifter data show such a broad weak southward current and also revealed large spatial variability and circulation patterns within the Portugal Current. The computation of 95% confidence error ellipses indicates these meanders and eddies are persistent features of the Portugal Current. Large-scale wave patterns and zonal variability were also found in numerical experiments in this region [*Spall*, 1990].

A minor branch of the east extension of the Azores Current moves southward near 22°W and joins the Canary Current near 30°N, 20°W, northwest of the Canary Islands. The current barrier formed by the Madeira Plateau is a robust result of these features. Large numbers of drifters passed around the area during the nearly 4-year period. The "hole" left by this bifurcation process is clearly seen in the composite trajectories in Figure 2. Historical observations of the large-scale dynamic height field in the area show the general anticyclonic sweep of surface currents in the vicinity of the Madeira Plateau [e.g., *Käse et al.*, 1986; *Stramma*, 1984], but the details visible in these drifter observations have not been seen before.

The Canary Current revealed by drifter data is confined within a much narrower band than a broad scale in climatological data set [*Robinson et al.*, 1979; *Spall*, 1990]. There are hardly any drifters crossing 4000 m isobath, which implies the existence of a front which separates the central gyre water from the coastal water.

Utilizing the drifter data, ECMWF wind fields and the empirical formula of wind-driven currents, we obtained the best least squares fit of the relative sea level from the momentum equations for further illustrating the Azores Current and the Canary Current. On the left-hand side of (10) the order of the first term is of 10^{-5} cm s^{-1}, and the order of the second term is of 10^{-4} cm s^{-1}. On the right-hand side of (10) the order of the second term is of 10^{-4} cm s^{-1}. Our calculated sea level gradient is of the same order of 10^{-4} cm s^{-1}. Thus the first order of force balance has to be between the Coriolis force, the sea level gradient, and the vertical gradient of shear stress.

Using β and θ equal to 0.02 and 52.7° obtained by minimizing the least squares error ε^2, we have ε^2 equal to 1.3×10^{-13}. This leads to the standard deviation of the residual error equal to 3.6×10^{-7}, which is 10^{-3} times smaller than the first-order terms in (10). Hence this error is insignificant after minimizing. The dominant errors in the sea level estimates should come from the error fields of mean flow and the wind field. From (10), we can directly estimate the error induced by the error of mean flow, that is, the error of seal level is equal to the error of mean flow multiplied by a factor of $(f\cdot\Delta x/g)$, where Δx is the scale of the subregion. Taking Δx

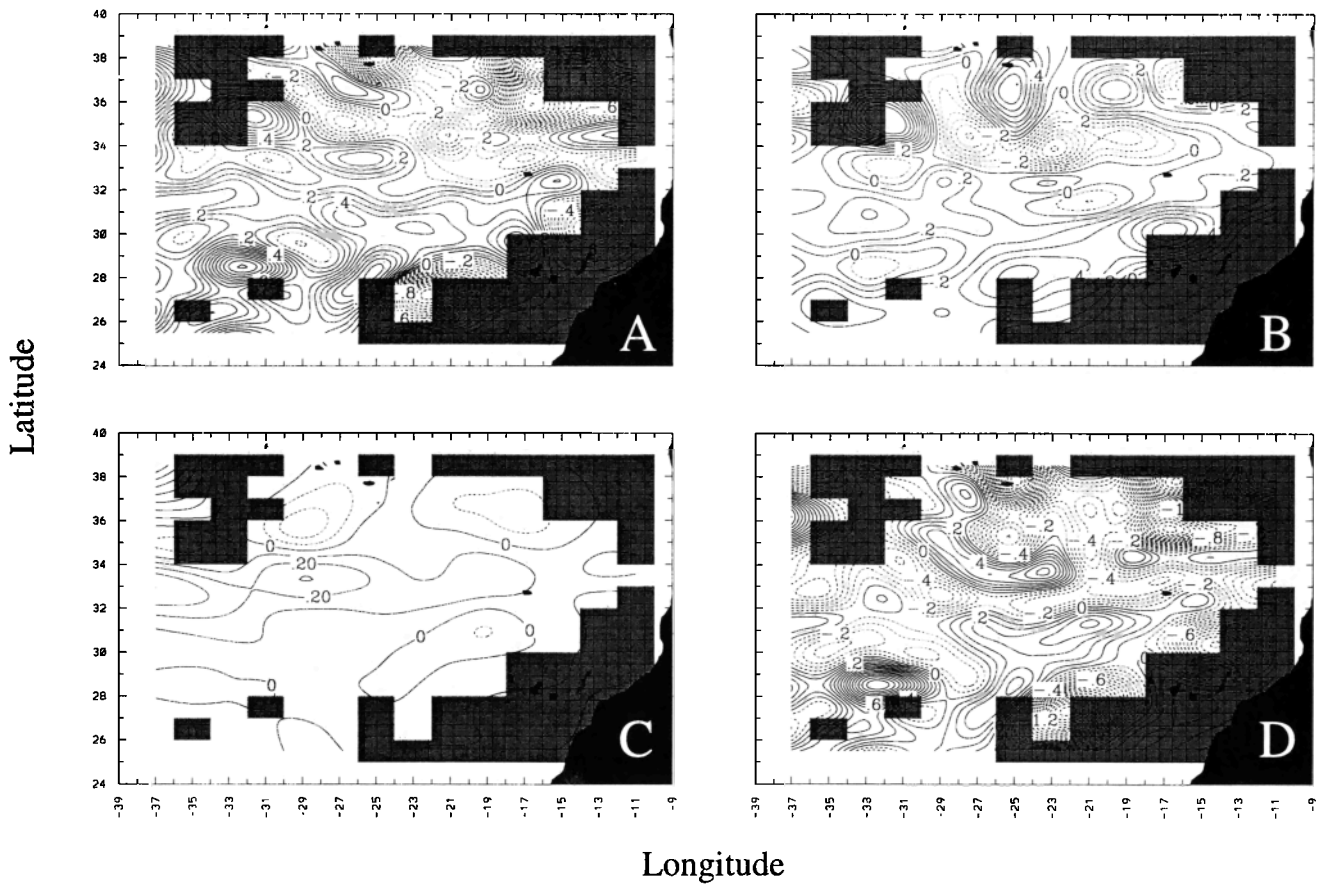

Figure 16. (a) Estimates $\rho c_p[\langle dT/dt\rangle-\langle \partial T/\partial t\rangle]$ (W m^{-3}), (b) $-\rho c_p\langle \mathbf{u}\rangle\cdot\langle \nabla T\rangle$ (W m^{-3}), (c) $-\rho c_p\nabla\cdot\langle \mathbf{u}'T'\rangle$ (W m^{-3}), and (d) the heat subduction, $\rho c_p\partial\langle T'w'\rangle/\partial z$ (W m^{-3}). The contour interval is equal to 0.1 (W m^{-3}).

equal to 200 km, we have the error of the relative sea level equal to 2.6×95% confidence interval of the mean current (Figure 8b), which varies from 2 to 6 cm in the Azores Current and the Canary Current.

The highest gradient of sea level near 33°-35°N is consistent with the Azores Current, which is constrained within a much narrower range than the front zone shown from the climatological data [*Robinson et al.*, 1979] and Geosat altimeter data [*Le Traon and De Mey*, 1994]. We found that the southwestward Canary Current is also confined on the narrow continental slope rather than a broad flow [*Käse et al.*, 1986]. The sea level map also revealed the general anticyclonic circulation of the surface currents in the vicinity of the Madeira Plateau. North and south of the Azores Current there are gradients of sea level associated with westward flowing countercurrents.

7.2. Eddy Kinetic Energy

EKE levels shown in Figure 9 attain maximum values of ~200 $cm^2 s^{-2}$ along the Azores Current, reflecting eddy velocities of approximately 14 cm s^{-1}. Thus the magnitude of eddy velocities is similar to that of the mean currents, which is unusual for open ocean surface currents. This suggests that mesoscale eddies generated locally through undulations and pinching off of the current dominate the eddy activity in the Azores Current, as observed also in the Gulf Stream. The scale of mesoscale eddies can be examined by the Eulerian transversal correlation, which is associated with rotational motion of meanders and eddies. In our study area the dominant spatial scale is approximately equal to 100 km and 140 km in the zonal and meridional directions, respectively. Thus the bin size of 1°×2° is ideal for the EKE produced by meanders of the Azores Current.

In sharp contrast, EKE values in the Canary Current are lower by half than the Azores Current (<100 $cm^2 s^{-2}$). There is a tongue toward the southwest which originates at the east extension of the Azores Current. The Canary Current is relatively steady. It is likely that it is strongly controlled by the continental slope off northwest Africa and relatively few (or weak) mesoscale eddies are generated within it.

The zonally averaged zonal currents show clearly the locations of the Azores Current and the peak of EKE, that the peak of EKE occurs along the principle axis of the Azores Current (Figure 9b). In the study of mesoscale eddies in the Canary Basin, *Rudnick* [1996] indicated that there are more variabilities beneath the thermocline at the warm side of a front due to the intrusion of relative heavy water from the cold side of the front. Our results do not show this feature because the spatial average in this study eliminates such detailed spatial feature. Instead, EKE decreases rather more sharply south of the Azores Current than that north of the Azores Current. If the surface warm water spins off and translates northward, and the southward intrusion of cold water presents more likely beneath the thermocline, the surface EKE should be more energetic north of the Azores Current. This result is consistent with the results from the Geosat altimeter reported by *Le Traon and De Mey* [1994]. The maximum variability of sea level anomalies from their 2-year data set (November 1986 to December 1988) was found along 34.5°N, generally north of the axis of the Azores Current.

How is the eddy kinetic energy produced? To answer this question, we investigated each term in the eddy kinetic energy equation (15). Conceptually, the mesoscale eddies associated with flow instabilities are responsible to EKE. However, our computation indicates that work done by fluctuations of sea surface slopes and wind stress on those velocity components which are not under geostrophic and Ekman balance are partially responsible for the eddy motion in this region (Figure 11a). The contribution of random wind to EKE production is positive in most of our study region except for a negative band northwest of the Madeira Island. The highest variation occurs in the region of the Azores Current, although it is relatively smoother than the other two terms directly determined by mesoscale dynamics.

The maximum of energy transfer from the mean Azores Current by Reynolds stress occurred at 34°N, 28°W, south of the current where an eddy kinetic energy maximum was also found. Within the eastern extension of the Azores Current and the Canary Current, Reynolds stress plays the opposite role which transfers the energy from random motion to the mean currents (34°N, 21°W). The nature of isotropic eddy fields in this study area leads to the positive correlation between the mean current convergence and work done on the mean current by Reynolds stress. The convergence of the mean current determines the direction of the energy flux between mean and eddy fields (i.e., equation 17). In the subduction area an eddy will be stretched and kinetic energy will be released to the mean current.

7.3 Heat Advection

Based on the climatological data, *Stramma and Isemer* [1988] estimated both geostrophic and Ekman temperature fluxes from 0 to 1000 m depth and from 0 to 50 m, respectively, between 35°W and the African and European coast. The total temperature flux varies from -0.2×10^{15} W at 40°N, -0.7×10^{15} W at 30°N, to -0.5×10^{15} W at 25°N. The Ekman temperature flux varies from -0.1×10^{15} W at 40°N, 0.05×10^{15} W at 30°N, to 0.2×10^{15} W at 25°N. Our estimate of the temperature flux from 0 to 50m depth is equal to -0.076 $\pm0.022\times10^{15}$ W, which differs from that estimated by *Stramma and Isemer* [1988]. Because Eulerian currents measured by drifters represent the sum of both geostrophic and ageostrophic velocity components, our estimated meridional temperature flux is the total temperature flux produced by both velocity components in the Ekman layer. This flux within 0-50 m depth makes up 10-20% of the total temperature flux between 1 and 1000 m depth estimated by *Stramma and Isemer* [1988].

The vertical turbulent heat flux through the bottom of an Ekman layer cannot be ignored because the mixed layer can be significantly deeper than the Ekman layer. Thus, after removing the seasonal temperature trends from drifter data, $\rho c_p[\langle dT/dt\rangle - \langle \partial T/\partial t\rangle]$ is proportional to the mean net heat flux between air-sea surface heat flux and heat flux through the bottom of the Ekman layer (Figure 16a). We can further express $\rho c_p[\langle dT/dt\rangle - \langle \partial T/\partial t\rangle]$ as

$$\rho c_p\left[\left\langle\frac{dT}{dt}\right\rangle-\left\langle\frac{\partial T}{\partial t}\right\rangle\right] = \rho c_p\left[\langle u\rangle\frac{\partial\langle T\rangle}{\partial x}+\langle v\rangle\frac{\partial\langle T\rangle}{\partial y}\right]+\rho c_p\left\langle u'\frac{\partial T'}{\partial x}+v'\frac{\partial T'}{\partial y}\right\rangle \quad (22)$$

which represents the total horizontal advective convergence processes of heat including the horizontal mesoscale eddy

contribution. A general cooling area extends eastward from 35°N, 28°W to the north of Madeira Island, and the Azores Current flows down the temperature gradient (Figure 16b). In the region of the Canary Current, the water is heated as it flows up the temperature gradient.

Taking the Ekman layer depth of 50 m, the heating rate is 20 W m^{-2} near the African and European coast corresponding to the contour of 0.4 W m^{-3} in Figure 16a. A maximum is located at 31°N, 27°W. If we can estimate the mixed layer depth and assume the heat flux through the stratification can be ignored, we can estimate the surface heat flux into the mixed layer. If the mixed layer depth varies from 50 to 100 m in this area, the surface heat flux should be 1-2 times larger than the estimates in Figure 16a. Estimates of the surface heat flux in this region from other observations or from atmospheric general circulation models are comparable to these values [e.g., *Bunker*, 1976; *Isemer et al.*, 1989; *Gulev*, 1995]. This drifter data set may perhaps provide the most accurate resource to derive surface heat fluxes of the sum of the turbulent and radiation heat.

Comparing estimates of convergence and heating anomaly ($\rho c_p[\langle dT/dt\rangle - \langle \partial T/\partial t\rangle]$), we can find consistent patterns between the areas of positive work done by Reynolds stress, subduction, and cooling anomaly north of the Azores Current (Figures 11b, 12b, and 16a). We should point out that the calculation of heating anomaly is completely independent of the velocity calculation. This consistency leads us to think that the warmer water is advected down the temperature gradient in the Azores Current. As it is cooled it subducts, meanwhile releasing the mean kinetic energy to the eddy field. These observations conflict with the subduction hypothesis that the subduction is driven by coupled local cooling convection and Ekman pumping [*Luyten et al.*, 1983; *Huang*, 1990].

In (21), the horizontal heat transport in the Ekman layer produced by both horizontal advection and diffusion is of the same order of the vertical heat flux through air-sea surface. Noticing that T is nearly uniform in the mixed layer, the last term in (21) can be written approximately as

$$\left\langle T' \frac{\partial w'}{\partial z} \right\rangle \approx \frac{\partial \langle T'w' \rangle}{\partial z} \tag{23}$$

which represents the vertical heat flux produced by the vertical motion associated with mesoscale eddies. By integrating (21) and (23) vertically through the Ekman layer and rearranging, we have

$$\begin{aligned} -\rho c_p \langle T'w'_b \rangle = \rho c_p H \left[\left\langle \frac{dT}{dt} \right\rangle - \left\langle \frac{\partial T}{\partial t} \right\rangle \right] \\ - \left[\langle u \rangle \frac{\partial \langle T \rangle}{\partial x} + \langle v \rangle \frac{\partial \langle T \rangle}{\partial y} \right] \\ - \left[\frac{\partial \langle u'T' \rangle}{\partial x} + \frac{\partial \langle v'T' \rangle}{\partial y} \right] \end{aligned} \tag{24}$$

where w'_b represents the vertical velocity of mesoscale eddies at the bottom of an Ekman layer, and then, $-\rho c_p \langle T'w'_b \rangle$ represents the downward heat flux produced by this vertical velocity. Using the estimates of surface heating and horizontal heat transports, we can infer the vertical heat flux through the bottom of an Ekman layer. This vertical heat flux is associated with the mesoscale eddy fields, which represents a different subduction process from the mean current subduction. The negative values in Figure 16 represent the typical cold water subduction associated with the eddy motion. There are two positive value regions around the Azores Current and Canary Current, indicating the warm water subduction or cold water upwelling.

7.4. Summary

The multiyear drifter data provide a statistically meaningful description of the Azores Current associated with the subtropical convergence zone at 34°N with the typical speed of 10-15 cm s^{-1}. It bifurcates around 22°W with the major branch of the current circling the Madeira Plateau and joining the Canary Current along the continental slope. The Azores and Canary Currents are constrained within narrower bands where large gradients of sea level exist. Westward countercurrents on both sides of the Azores Current are evidenced. The divergence field of array bias-corrected mean currents reveals a region of maximum convergence north of the Azores Current.

The eddy field revealed by drifter data has a timescale of 16 days and a spatial scale of 100-140 km. Both diffusivity and Reynolds stress are dominated by diagonal elements and weakly depart from being isotropic. Eddy kinetic energy maxima are found along the negative vorticity (southern) side of the Azores Current. There is a strong correlation between the divergence and work done by Reynolds stress. Because Reynolds stress is nearly isotropic, the sign of divergence determines the direction of energy transfer between mean and eddy fields. Utilizing the nearly isotropic property of Reynolds stress provides a new method to estimate the divergence field from drifter data.

The southward meridional temperature flux in the Ekman layer (0-50 m) between 37°W and the African and European coast is found at approximately -0.076 $\pm 0.022 \times 10^{15}$ W, produced by mean southward volume transport in our study area. The estimated surface heat flux and horizontal heat fluxes within the Ekman layer produced by advection and diffusion are of the same order. The water advected eastward in the Azores Current is cooled and subducts as it releases its mean kinetic energy to eddy fields. The residual between surface heating and horizontal heat flux must be balanced locally by the vertical flux associated with the vertical velocity of mesoscale eddies, which leads to a cold water subduction when this value is negative and a cold water upwelling when this value is positive. This subduction also occurs along the northern side of the front. This may elucidate a subduction process associated with mesoscale temperature and flow fields, which is different from the subduction of mean currents.

Acknowledgments. This research was supported by Office of Naval Research grants N00014-90-J-1788 and N00014-93-WR-24010. W. Krug and M. Pazos of NOAA/AOML in Miami were instrumental in deploying drifters and processing the drifter data, respectively. P. Blouch and J Rolland provided data from the French Bodega drifters along with helpful discussions. Authors would like to thank two anonymous reviewers for their critical comments.

References

Beyer, W H., *Handbook of Mathematical Sciences*, 859 pp., CRC Press, Boca Raton, Fla., 1987.

Bunker, A.F., Computations of surface energy flux and annual air-sea interaction cycles of the North Atlantic Ocean, *Mon. Weather. Rev.*, *104*, 1120-1140, 1976

Caniaux, G, and S. Planton, A three-dimensional ocean mesoscale simulation using data from the SEMAPHORE experiment: Mixed layer heat budget, *J. Geophys. Res*, *103*, 25,081-25,099, 1998.

Cromwell, D., P G Challenor, and A.L. New, Persistent westward flow in the Azores Current as seen from altimetry and hydrography, *J. Geophys Res*, *101*, 11923-11933, 1996.

Cushman-Roisin, B., Subduction, in Dynamics of the Oceanic Surface Mixed Layer, in *'Aha Huliko'a, Hawaiian Winter Workshop*, Hawai. Inst of Geophys. Spec Publ., edited by P. Müller and D. Henderson, pp. 181-196, Univ. of Hawaii at Manoa, 1987.

Davis, R.E., Observing the general circulation with floats, *Deep Sea Res.*, *38*, suppl 1, S531-S571, 1991.

de Szoeke, R.A., On the effects of horizontal variability of wind stress on the dynamics of the ocean mixed layer, *J. Phys. Oceanogr.*, *10*, 1439-1454, 1980.

Eymard, L., Introduction: The SEMAPHORE experiment, *J. Geophys. Res.*, *103*, 25,005-25,008, 1998.

Eymard, L., et al, Study of the air-sea interactions at the mesoscale: The Semaphore experiment, *Ann Geophys.*, *14*, 986-1015, 1996.

Federiuk, J.M, and J.F Price, Subduction mechanisms in the North Atlantic, *Eos Trans. AGU*, *65*, 943, 1984.

Giannetti, P., The velocity field in the northeast Atlantic from satellite-tracked drifting buoys, Master thesis, Nav. Postgraduate Sch, Monterey, Calif., 1993.

Gould, W.J., Physical oceanography of the Azores Front, *Prog. Oceanogr.*, *14*, 167-190, 1985.

Gulev, S K., Long-term variability of sea-air heat transfer in the North Atlantic Ocean, *Int. J. Climatol.*, *15*, 825-852, 1995.

Hansen, D.V., and P.M. Poulain, Quality control and interpolations of WOCE-TOGA drifter data, *J. Atmos. Oceanic. Technol.*, *13*, 900-909, 1996

Hoskins, B.J., I Draghici, and H.C. Davis, A new look at the ω-equation, *Q. J. R Meteorol. Soc*, *104*, 31-38, 1978.

Huang, R.X., Matching a ventilated thermocline model with inertial western boundary currents, *J. Phys. Oceanogr.*, *20*, 1599-1607, 1990.

Inoue, E., On the turbulenct diffusion in the atmosphere, *J. Meteorl. Soc. Japan*, *28*, 441-456, 1950.

Isemer, H.-J., and L. Hasse, *The Bunker Climate Atlas of the North Atlantic Ocean, vol 2, Air-Sea Interactions*, 252 pp., Springer-Verlag, New York, 1987.

Isemer, H.-J, J. Willebrand, and L. Hasse, Fine adjustment of large scale air-sea energy flux parameterizations by direct estimates of ocean heat transport, *J Clim.*, 2, 1173-1184, 1989.

Kase, R.H., and G. Siedler, Meandering of the subtropical front southeast of the Azores, *Nature*, *300*, 245-246, 1982.

Kase, R.H., W. Zenk, T.B. Sanford, and W. Hiller, Currents, fronts and eddy fluxes in the Canary Basin, *Prog. Oceanogr.*, *14*, 231-257, 1985.

Käse, R H., J.F. Price, P.L. Richardson, and W. Zenk, A quasi-synoptic survey of the thermocline circulation and water mass distribution within the Canary Basin, *J. Geophys. Res.*, *91*, 9739-9748, 1986.

Klein, B., and G. Siedler, On the origin of the Azores Current, *J. Geophys. Res.*, *94*, 6159-6168, 1989.

Krauss, W, and R H. Käse, Mean circulation and eddy kinetic energy in the eastern North Atlantic, *J Geophys. Res.*, *89*, 3407-3415, 1984.

Kwon, B.H., A Druilhet, H. Giordani, S. Planton, B. Benech, D. Lambert, and P. Durand, Structure of the marine atmospheric boundary layer over an oceanic thermal front: SEMAPHORE experiment, *J. Geophys. Res.*, *103*, 25,159-25,180, 1998.

Le Traon, P.Y., and P. De Mey, The eddy field associated with the Azores front east of the mid-Atlantic ridges as observed by the Geosat altimeter, *J Geophys. Res.*, *99*, 9907-9923, 1994.

Luyten, J.R., J. Pedlosky, and H. Stommel, The ventilated thermocline, *J. Phys Oceanogr.*, *13*, 292-309, 1983.

Monin, A S, and A.M. Yaglom, *Statistical Fluid Mechanics: Mecahnicas of Turbulence*, 769 pp., The MIT Press, Cambridge, Massachusetts, and London, England, 1971.

Niiler, P P, and R.W. Reynolds, The three-dimensional circulation near the eastern north Pacific subtropical front, *J. Phys. Oceanogr.*, *14*, 217-230, 1984

Niiler, P.P, R.E Davis, and H.J. White, Water-following characteristics of a mixed layer drifter, *Deep Sea Res.*, *34*, 1867-1881, 1987.

Niiler, P.P., A.S. Sybrandy, K Bi, P.-M. Poulain, and D. Bitterman, Measurements of the water-following capability of Holey-sock and TRISTAR drifters, *Deep Sea Res.*, *42*, 1951-1964, 1995.

Nurser, A.J.G., and J.C. Marshall, On the relationship between subduction rates and diabatic forcing of the mixed layer, *J. Phys. Oceanogr.*, *21*, 1793-1802, 1991.

Ogura, Y., The theory of turbulent diffusion in the atmosphere, *J. Meteorl. Soc. Japan*, *30*, 23-28, 1952.

Paduan, J D., and P P. Niiler, Structure of velocity and temperature in the northeast Pacific as measured with Lagrangian drifters in fall 1987, *J. Phys Oceanogr.*, *23*, 585-600, 1993.

Pedlosky, J, *Geophysical Fluid Dynamics*, 624 pp., Springer-Verlag, New York, 1987.

Pollard, R T, and R Millard, Comparison between observed and simulated wind-generated inertial oscillations, *Deep Sea Res.*, *17*, 813-821, 1970

Pollard, R.T, and S. Pu, Structure and circulation of the upper Atlantic Ocean northeast of the Azores, *Prog. Oceanogr.*, *14*, 443-462, 1985.

Pollard, R T., and L.A. Regier, Large variations in potential vorticity at small spatial scales in the upper ocean, *Nature*, *348*, 227-229, 1990.

Pollard, R.T., and L A. Regier, Vorticity and vertical circulation at an ocean front, *J Phys. Oceanogr*, *22*, 609-625, 1992.

Poulain, P., and P.P. Niiler, Statistical analysis of the surface circulation in the California Current system using satellite-tracked drifters, *J. Phys. Oceanogr.*, *19*, 1588-1603, 1989.

Ralph, E.A., and P.P. Niiler, Wind-driven currents in the tropical Pacific, *J Phys. Oceanogr.*, *29*, 2121-2129, 1999.

Reynolds, R.W. and T.M. Smith, Improved global sea surface temperature analyses, *J. Clim.*, *7*, 929-948, 1994.

Reynolds, R.W., and T.M. Smith, A high-resolution global sea surface temperature climatology, *J. Clim.*, *8*, 1571-1583, 1995.

Richardson, P L., and A. Tychensky, Meddy trajectories in the Canary Basin measured during the SEMAPHORE, *J. Geophys. Res*, *103*, 25,029-25,046, 1998.

Robinson, M.K., R.A. Bauer, and E.H. Schroeder, Atlas of North Atlantic-Indian Ocean monthly mean temperature and mean salinities of the surface layer, Ref Publ. 18, U.S. Nav. Oceanogr. Off., Washington, D C, 1979

Rudnick, D.L, Intensive surveys of the Azores Front, 2, Inferring the geostrophic and vertical velocity fields, *J. Geophys. Res.*, *101*, 16291-16303, 1996.

Rudnick, D L, and J.R. Luyten, Intensive surveys of the Azores Front, 1, Tracers and dynamics, *J. Geophys. Res.*, *101*, 923-939, 1996.

Saunders, P M., Circulation in the eastern North Atlantic, *J. Mar. Res.*, *40*, 641-657, 1982.

Simmon, A J., and D. Dent, The ECMWF multi-tasking weather prediction, *Comput. Phys. Rep.*, *11*, 165-194, 1989.

Spall, M A, Circulation in the Canary Basin: A model/data analysis, *J. Geophys. Res.*, *95*, 9611-9628, 1990.

Stramma, L., Geostrophic transport in the warm water sphere of the eastern subtropical North Atlantic, *J. Mar. Res.*, *42*, 537-558, 1984.

Stramma, L., and H.-J. Isemer, Seasonal variability of meridional temperature fluxes in the eastern North Atlantic Ocean, *J. Mar. Res.*, *46*, 281-299, 1988.

Stramma, L., and T.J. Müller, Some observations of the Azores Current and the North Equatorial Current, *J. Geophys. Res.*, *94*, 3181-3186, 1989.

Sverdrup, H.U., U.W. Johnson, and R.H. Flemming, *The Oceans*, 1087 pp, Prentice-Hall, Englewood Cliffs, N. J., 1942.

Swenson, M S., and P.P. Niiler, Statistical analysis of the surface circulation of the California Current, *J. Geophys. Res.*, *101*, 22,631-22,645, 1996

Sybrandy, A.L., and P P. Niiler, WOCE/TOGA Lagrangian drifter construction manual, *SIO Ref. 91/6*, Scripps Inst. of Oceanogr., Univ. of Calif, San Diego, 1991.

Taylor, G.I., Diffusion by continuous movements, *Proc. London. Math. Soc.*, *20*, 165-212, 1921.

Tychensky, A., P -Y. Le Traon, F. Hernandez, and D. Jourdan, Large structures and temporal change in the Azores Front during the SEMAPHORE experiment, *J. Geophys. Res.*, *103*, 25,009-25,028, 1998

P.P Niiler, Scripps Institution of Oceanography, University of California, San Diego, La Jolla, CA 92093.

J D. Paduan, Department of Oceanography, Naval Postgraduate School, Monterey, CA 93943

M. Zhou, Department of Physics, Large Lakes Observatory, University of Minnesota, 213 Research Laboratory Building, 10 University Drive, Duluth, MN 55812. (mzhou@d.umn.edu)

(Received December 30, 1998; revised February 24, 2000;
accepted April 3, 2000)